

Crystalline symmetry protected Majorana mode in number-conserving Dirac semi-metal nanowires

Rui-Xing Zhang¹ and Chao-Xing Liu¹

¹*Department of Physics, The Pennsylvania State University, University Park, Pennsylvania 16802*
(Dated: April 22, 2022)

One of the cornerstones for topological quantum computations is Majorana zero mode, which has been intensively searched in fractional quantum Hall systems and topological superconductors. Several recent works suggest that such exotic mode can also exist in one dimensional (1D) interacting double-wire setup even without long-range superconductivity. A notable instability in these proposals comes from inter-channel single-particle tunneling that spoils the topological ground state degeneracy. Here we show that 1D Dirac semimetal (DSM) nanowire is an ideal number-conserving platform to realize such Majorana physics. By inserting magnetic flux, a DSM nanowire is driven into 1D crystalline-symmetry-protected semimetallic phase. Interaction enables the emergence of boundary Majorana zero modes, which is robust as a result of crystalline symmetry protection. We also explore several experimental consequences of Majorana signals.

Introduction - Anyons are natural generalizations of bosons and fermions from the perspective of quantum statistics. Interchanging a pair of anyons can induce either a non-trivial phase factor $e^{i\theta} \neq \pm 1$ in the wavefunction (Abelian anyons), or a rotation operation of the corresponding many-body wave function among a degenerate set of locally indistinguishable states (non-Abelian anyons) [1]. Anyonic physics was first pointed out in the context of fractional quantum Hall (FQH) effect [2], where anyons emerge as bulk quasiparticle excitations in an FQH system. A well-known example here is Majorana quasiparticle (Ising anyon), which emerges in a $\nu = \frac{5}{2}$ Moore-Read FQH state [3]. The non-Abelian statistics of Majorana quasiparticle makes it a promising candidate for building a topological quantum computer [4]. Besides FQH systems, Majorana physics was also studied in the topological superconductor (TSC) after the pioneering works by Read and Green [5], Ivanov [6] and Kitaev [7]. In particular, Kitaev pointed out the existence of boundary Majorana zero mode (MZM) in a one-dimensional (1D) p-wave TSC. Such TSC is topologically distinct from a conventional superconductor due to the MZM-induced ground state degeneracy (GSD) [8]. The degenerate ground states are further labeled by Z_2 fermion parity of the system, and their stability is guaranteed by this Z_2 parity symmetry. This Kitaev model serves as the underlying mechanism of recent intensive experimental efforts in realizing MZM physics in 1D semiconductor devices [9–14].

Theoretically, it was pointed out that MZM will become unstable in a single 1D quantum wire if strong quantum fluctuations destroy long-range superconductivity [15]. For a double-wire setup, however, MZMs can coexist with quantum fluctuations when inter-wire single-particle hopping vanishes while pair hopping interaction dominates [15–24]. Pair hopping process fluctuates particle number of each quantum wire only by a multiple of 2. Thus in each quantum wire, an emergent Z_2 fermion parity $P^{(2)}$ is well defined. Consequently, $P^{(2)}$ defines dou-

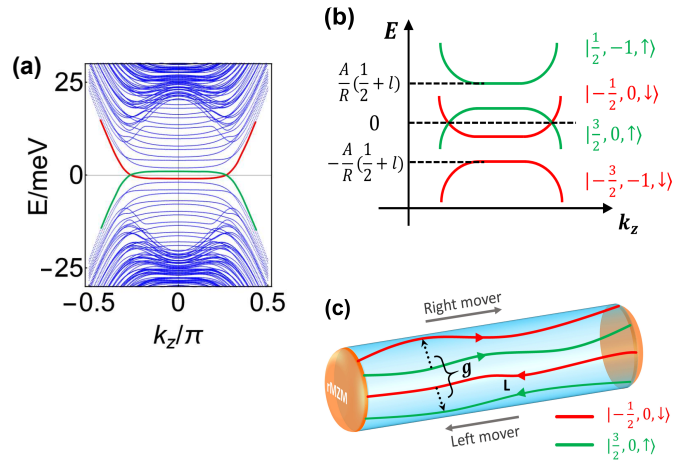


FIG. 1. In (a), DSM nanowire is driven into a rotation-symmetry-protected 1D semimetal when flux $\Phi = l\Phi_0$ ($\frac{1}{2} < l < \frac{3}{2}$) is inserted. The emerging 1D Dirac points originate from $|\frac{3}{2}, 0, \uparrow\rangle$ (green line) and $|\frac{1}{2}, 0, \downarrow\rangle$ (red line), as shown in (b). In (c), we show the process of pair-hopping interaction g , where two “red” electrons hop to the “green” electron states simultaneously. This process respects four-fold rotation symmetry, and enables the emergence of Majorana end states.

bly degenerate ground states, which mimics the physics in Kitaev model. However, a well-known issue in the double-wire setup comes from “ Z_2 parity breaking” induced by inter-wire single particle tunneling, which is generally unavoidable. Such tunneling process explicitly violates $P^{(2)}$ symmetry and thus spoils Majorana physics.

In this work, we demonstrate how crystalline symmetries naturally solve the “ $P^{(2)}$ breaking” issue, and thus stabilize the Majorana physics without long-range superconductivity. We show that 1D nanowire of three dimensional Dirac semimetals (DSM) [25, 26] possesses crystalline-symmetry-protected gapless Dirac points, offering us a material realization of stable semimetallic phase (Fig. 1 (a)). Therefore, a DSM nanowire man-

ifests itself as an effective double-wire setup, with each “quantum wire” labeled by a representation of the crystalline symmetry group. Inter-“wire” pair-hopping interaction drives the system into an interaction-enabled topological phase with doubly degenerate ground states and MZMs (Fig. 1 (c)). On the other hand, the origin of $P^{(2)}$ -breaking, inter-“wire” *single*-particle tunneling, is forbidden in our rotation-invariant system, since it explicitly breaks the rotation symmetry. As a result, *rotational symmetry protects the robustness of the Majorana physics in the DSM nanowire system*. The boundary MZM in our setup bridges between ground states with different angular momentum representations of the rotational crystalline group. It is thus dubbed “representation MZM” (rMZM) to distinguish from conventional MZMs in TSCs. Experimentally, rMZM is shown to exhibit exponentially localized zero-bias peak signal, which can be detected via scanning tunneling microscopy (STM). We also propose a feasible setup to explore the transport physics of rMZM, where the transport phase diagram and experimental signals are discussed.

1D Dirac points in DSM nanowires - The following $k \cdot p$ Hamiltonian describes a typical DSM protected by the C_4 symmetry[25, 26]

$$H_{k \cdot p} = \begin{pmatrix} M(k) & Ak_- & 0 & 0 \\ Ak_+ & -M(k) & 0 & 0 \\ 0 & 0 & -M(k) & -Ak_- \\ 0 & 0 & -Ak_+ & M(k) \end{pmatrix}, \quad (1)$$

The basis function Ψ is $(|P, \frac{3}{2}\rangle, |S, \frac{1}{2}\rangle, |S, -\frac{1}{2}\rangle, |P, -\frac{3}{2}\rangle)^T$, where spin-orbit-coupled angular momentum $J \in \{\pm\frac{1}{2}, \pm\frac{3}{2}\}$ acts as a pseudo-spin index. Notice that $H_{k \cdot p}$ takes a block-diagonal form of $\text{diag}(H_\uparrow, H_\downarrow)$, with each block describing a Weyl Hamiltonian in the corresponding spin (\uparrow or \downarrow) sector. Here $M(k) = M_0 - M_1 k_z^2 - M_2(k_x^2 + k_y^2)$ and $k_\pm = k_x \pm ik_y$, with $A > 0$ and $M_{0,1,2} > 0$. The bulk Dirac points are aligned along rotational invariant k_z axis at $k_z = \pm\sqrt{M_0/M_1}$. The \uparrow and \downarrow sectors are related via $H_\downarrow(M(k), A) = H_\uparrow(-M(k), -A)$. Thus, we will focus on H_\uparrow , and the properties of H_\downarrow can be obtained analogously.

The DSM nanowire can be better described in cylindrical coordinates. We rewrite H_\uparrow in terms of $k_r = -i\partial_r$ and $k_\theta = -\frac{i}{r}\partial_\theta$ with angular variables $r = \sqrt{x^2 + y^2}$ and $\theta = \arctan \frac{y}{x}$. Solving the eigen-state problem [27], the low-energy eigenstates of H_\uparrow are found to be Fermi arc states on the side surface of the nanowire [28]. For a nanowire with radius R , surface Fermi arc spectrum $E_\uparrow = -\frac{A}{R}(m + \frac{1}{2})$, where $m = 0, \pm 1, \pm 2, \dots$ is the eigenvalue of k_θ . The spin-down part of H_0 behaves similarly with $E_\downarrow = \frac{A}{R}(m + \frac{1}{2})$. Notice that the complete Fermi arc spectrum always exhibits a finite gap of A/R , which originates from the π spin Berry phase of the Fermi arc states [29]. In this nanowire geometry, total angular momentum J_{tot} is a good quantum number, while it is ac-

tually composed of two parts: (1) angular contribution from k_θ and (2) pseudo-spin J which is encoded in the basis Ψ . In particular, we find that a state with $k_\theta = m$ carries $J_{tot} = m + 2\sigma + \frac{1}{2}$ in the spin- σ ($\sigma = \pm\frac{1}{2}$) sector. Thus, we label an energy eigen-state as $|J_{tot}, m, \sigma\rangle$ where spin index $\sigma \in \{\uparrow, \downarrow\}$.

The 1D Dirac points can be realized by inserting magnetic flux to remove the Berry phase effect. The applied magnetic field should be precisely aligned along the nanowire to preserve the C_4 symmetry. With flux $\Phi = l$ (in units of $\Phi_0 = h/e$) inserted, $E_{\uparrow/\downarrow} = \mp\frac{A}{R}(m + \frac{1}{2} - l)$. The π Berry phase is exactly canceled, when π -flux ($l = \frac{1}{2}$) is inserted. Consequently, $|\frac{3}{2}, 0, \uparrow\rangle$ touches $|-\frac{1}{2}, 0, \downarrow\rangle$ at $k_z = 0$, which is similar to the worm-hole effect of topological insulator nanowire [30]. When Φ is further increased, $|\frac{3}{2}, 0, \uparrow\rangle$ intersects with $|-\frac{1}{2}, 0, \downarrow\rangle$ to form a gapless inverted band structure (1D Dirac points), as shown in Fig. 1 (b). Since $|\frac{3}{2}, 0, \uparrow\rangle$ and $|-\frac{1}{2}, 0, \downarrow\rangle$ belong to different representations of the rotational group, the 1D Dirac points are robust and thus protected by C_4 symmetry. In Fig. 1 (a), we verify the above results in the tight-binding model obtained from regularizing the $k \cdot p$ Hamiltonian on a cubic lattice [31]. The magnetic field required for inducing 2π flux is around 1T for a nanowire with a diameter of 100 nm [27]. This is how we assemble a 1D rotation-symmetry-protected semimetal by inserting magnetic flux into the DSM nanowire.

Interaction-induced Majorana physics - The low-energy theory of 1D Dirac points is well captured by the 2-channel Luttinger liquid (LL) theory,

$$H_0 = \sum_{s=1,2} \int dx \frac{v}{2} [\psi_{s,R}^\dagger(x) \partial_x \psi_{s,R}(x) - \psi_{s,L}^\dagger(x) \partial_x \psi_{s,L}(x)].$$

Here $\psi_{1,R(L)}^\dagger$ creates a right (left) moving electron with $J_{tot} = -\frac{1}{2}$, while $\psi_{2,R(L)}^\dagger$ creates a right (left) moving electron with $J_{tot} = \frac{3}{2}$. Two-particle processes that preserve both $U(1)$ charge conservation and C_4 rotation symmetry [32] are:

$$H_1 = \int dx [g\psi_{1,R}^\dagger\psi_{1,L}^\dagger\psi_{2,R}\psi_{2,L} + g_1\psi_{1,R}^\dagger\psi_{2,L}^\dagger\psi_{2,R}\psi_{1,L} + g_2\psi_{1,R}^\dagger\psi_{2,R}^\dagger\psi_{2,L}\psi_{1,L} + h.c.] \quad (2)$$

If we move the Fermi level slightly away from the Dirac points (zero energy in Fig. 1 (a) and (b)), both g_1 and g_2 scatterings involve certain amount of momentum transfer, and will be suppressed in a translational invariant system. Inter-channel pair-hopping g , however, preserves both momentum conservation and C_4 symmetry (angular momentum transfer $\Delta J_{tot} = 4$). As will be shown below, it is g that is responsible for Majorana physics.

We next apply Abelian bosonization technique [33] and define $\psi_{s,R} \sim e^{i\sqrt{\pi}(\phi_s - \theta_s)}$ and $\psi_{s,L} \sim e^{-i\sqrt{\pi}(\phi_s + \theta_s)}$ following the convention in [34]. It is convenient to introduce the bonding and anti-bonding fields as $\phi_\pm =$

$\frac{1}{\sqrt{2}}(\phi_1 \pm \phi_2)$ and $\theta_{\pm} = \frac{1}{\sqrt{2}}(\theta_1 \pm \theta_2)$, as well as K_{\pm} to be the Luttinger parameters for bonding and anti-bonding channel. The bonding sector remains gapless, while the anti-bonding sector might open up a non-trivial gap with the Hamiltonian

$$H_- = \int dx \frac{v}{2} [K_- (\partial_x \phi_-)^2 + \frac{1}{K_-} (\partial_x \theta_-)^2] + g \int dx \cos 2\sqrt{2\pi} \theta_- \quad (3)$$

We will focus on $K_- < 1$ where g is relevant under renormalization group analysis. At Luther-Emery point ($K_- = \frac{1}{2}$), Eq. 3 can be exactly mapped to the topological Kitaev model with MZM end states [16, 27]. Such mapping is achieved by refermionizing Eq. 3 with $\tilde{\psi}_R \sim e^{i\sqrt{\pi}(\tilde{\phi}-\tilde{\theta})}$ and $\tilde{\psi}_L \sim e^{-i\sqrt{\pi}(\tilde{\phi}+\tilde{\theta})}$, where $\tilde{\phi} = \phi_-/\sqrt{2}$ and $\tilde{\theta} = \sqrt{2}\theta_-$. Away from $K_- = \frac{1}{2}$, the above mapping fails while we will show that Majorana physics (both GSD and Majorana end states) persists.

The ground state is obtained by minimizing $\cos 2\sqrt{2\pi}\theta_-$ and pinning $\theta_- = (n_{\theta} + \frac{1}{2})\sqrt{\pi/2}$, where $n_{\theta} \in \mathbb{Z}$ is an integer-valued operator. Since θ_- has $\sqrt{2\pi}$ periodicity, there are two degenerate ground states $|\theta_- = \pm \frac{1}{2}\sqrt{\pi/2}\rangle$, which are characterized by the emergent Z_2 fermion parity $P^{(2)}$. Physically, $P^{(2)}$ counts the parity of electron number in the $J_{tot} = -\frac{1}{2}$ subspace,

$$P^{(2)} = (-1)^{\sqrt{\frac{1}{\pi}} \int_0^L dx \partial_x \phi_1} = P_+ P_- \quad (4)$$

where a nanowire with finite length L is considered and $P_{\pm} = e^{i\sqrt{\pi/2}(\phi_{\pm}(L) - \phi_{\pm}(0))}$. With $P^{(2)}\theta_-(P^{(2)})^{-1} = \theta_- - \sqrt{\pi/2}$, $P^{(2)}$ interchanges $|\theta_- = \pm \frac{1}{2}\sqrt{\pi/2}\rangle$ from one to another. Quantum superposition principle, however, allows us to define the following degenerate ground states,

$$|\pm\rangle = \frac{1}{\sqrt{2}} [|\theta_- = \frac{1}{2}\sqrt{\pi/2}\rangle \pm |\theta_- = -\frac{1}{2}\sqrt{\pi/2}\rangle], \quad (5)$$

where $|+\rangle$ and $|-\rangle$ are characterized by even and odd $P^{(2)}$ parity, respectively. Since $P^{(2)}$ is a global property of the system, the degeneracy here is topological, which can NOT be distinguished via any local measurement.

Topological GSD can also be revealed by constructing rMZM operators explicitly. Imposing open boundary condition at $x = 0$ gives rise to $\psi_{l,L}(0) + \psi_{l,R}(0) = 0$ for $l = 1, 2$, which corresponds to $\phi_l(0) = n_l^{(1)}\sqrt{\pi}$ up to an unimportant constant. Here, $n_l^{(1)} \in \mathbb{Z}$ is an integer-valued operator. Introducing $n_+^{(1)} = n_1^{(1)} + n_2^{(1)}$ and $n_-^{(1)} = n_1^{(1)}$, the boundary condition fixes the value of ϕ_{\pm} as $\phi_+(0) = n_+^{(1)}\sqrt{\pi/2}$ and $\phi_-(0) = (2n_-^{(1)} - n_+^{(1)})\sqrt{\pi/2}$. It is important to notice that $[n_-^{(1)}(x), n_{\theta}(x')] = \frac{i}{\pi}\Theta(x - x')$, while $n_+^{(1)}$ always commutes with n_{θ} and behaves like a c-number. Following Ref. [35], we construct rMZM op-

erator α_1 at $x = 0$ and α_2 at $x = L$ as,

$$\alpha_1 = e^{i\pi(n_-^{(1)} + n_{\theta})}, \quad (6)$$

$$\alpha_2 = e^{i\pi(n_-^{(2)} + n_{\theta})}, \quad (7)$$

where we have defined the boundary condition at $x = L$ to be $\phi_+(L) = n_+^{(2)}\sqrt{\pi/2}$ and $\phi_-(L) = (2n_-^{(2)} - n_+^{(2)})\sqrt{\pi/2}$ in a similar way. The Majorana properties of $\alpha_{1,2}$ can be easily checked, where $[\alpha_{1,2}, H_-] = 0$ and $\alpha_1^2 = \alpha_2^2 = 1$. Starting from a ground state $|+\rangle$, one can easily show that $\alpha_{1,2}|+\rangle = |-\rangle$ up to some phase factors. This also proves the topological GSD.

The essential role of C_4 symmetry in protecting rMZM should be emphasized. C_4 symmetry enforces inter-channel single-particle tunneling events to vanish as they break C_4 explicitly, which makes $P^{(2)}$ symmetry well-defined. Since $C_4\theta_-C_4^{-1} = \theta_- + \sqrt{\pi/2}$, it is easy to check that $C_4|\pm\rangle = \pm|\pm\rangle$, which proves $C_4 = P^{(2)}$. The equivalence between a N -fold discrete symmetry Z_N and an emergent Z_M fermion parity $P^{(M)}$ is a quite general result for two-channel systems, which is discussed in details in the supplementary materials [27].

We stress that our theory is not limited to the C_4 -symmetric DSM nanowire. For a 1D nanowire growing along the x direction, the crystalline structure in the cross-section (y - z plane) is characterized by a two-dimensional (2D) point group G_{2D} , where every symmetry operation in G_{2D} leaves the x direction invariant. Therefore, it is natural to generalize our theory from C_4 group to general 2D point groups. In [27], we identify simple criteria to determine whether a given symmetry group G could give rise to $P^{(2)}$ parity and present a complete discussion of all 2D point groups, as well as their double groups. In particular, our theory predicts all possible irreducible representations for each G_{2D} that could support Majorana physics, and thus establishes the guideline for the search of other candidate materials.

Experimental detection - One important approach to probe Majorana signals is to map out the spatial profile of spectral density using STM technique, and seek for exponentially localized zero-bias peak that originates from MZM bound state. Following this logic, we consider the single-electron-tunneling problem from a Fermi liquid lead to the DSM nanowire and seek for rMZM signals. This tunneling process changes both electron number and $P^{(2)}$ simultaneously. In particular, the ground state is changed from $|0\rangle = |N, p\rangle$ with N electrons and $P^{(2)} = p$ to $|1\rangle = |N + 1, -p\rangle$ with $N + 1$ electrons and $P^{(2)} = -p$ via this tunneling process. For a DSM nanowire at $x \in [0, L]$, in the $L \rightarrow \infty$ limit, transition matrix element of injecting a single electron at $x = x_0$ ($0 \leq x_0 \ll L$) can be calculated with the help of mode expansion technique [27, 36], and the resulting spectral density is

$$\rho(x, \omega \rightarrow 0) = |\langle 1 | \psi_{1,R}^{\dagger} | 0 \rangle|^2 = \mathcal{N}(x, \epsilon, K_{\pm}) e^{-\frac{\pi}{4K_-} \frac{x}{\epsilon}} \quad (8)$$

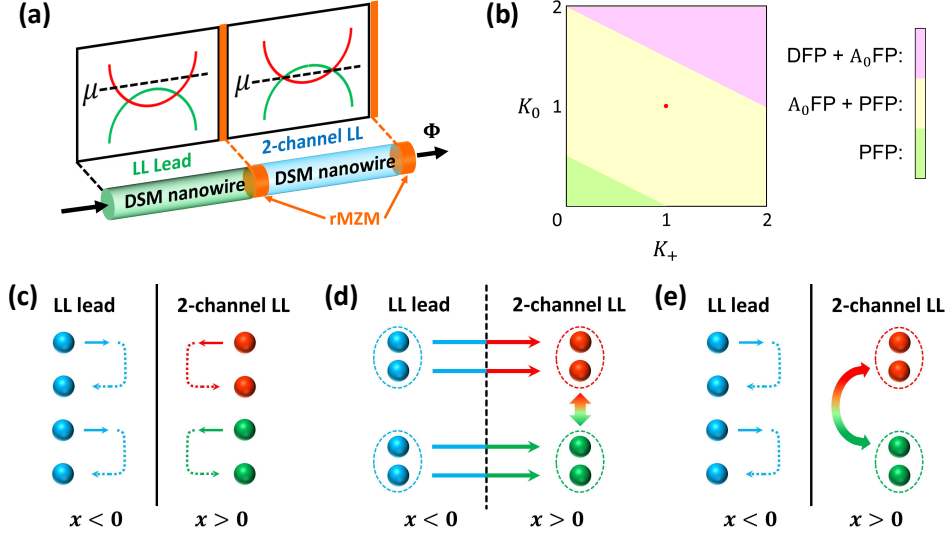


FIG. 2. (a) We apply a step-function gate to DSM nanowire to fabricate the 2LL/LL configuration. (b) Tunneling phase diagram of 2LL/LL junction with $K_- < 1$. In (c) - (e), we systematically plot the boundary conditions of the following fixed points: DFP, PFP and A_0 FP. The dashed circle that contains a pair of electrons signals pair-tunneling/backscattering process.

where $\xi = \sqrt{\frac{v}{8\pi g K_-}}$ is the correlation length of the system and ϵ is the short distance cut-off. While $\mathcal{N}(x, \epsilon, K_{\pm})$ counts the power-law contribution of this transition process [27], the exponential part of $\rho(x, \omega \rightarrow 0)$ unambiguously reveals an exponentially localized rMZM on the boundary, which is ready to be detected using STM technique. Since $\xi \sim 1/\sqrt{g K_-}$, the stronger the interaction, the more localized rMZM will be.

Finally, we consider a 2-channel LL/LL lead (2LL/LL) junction, which can be experimentally achieved by applying a step-function-like gating to the DSM nanowire, as shown in Fig. 2 (a). With this gating configuration, the right part of the nanowire ($x > 0$) is in the 2-channel LL regime, while the left part ($x < 0$) becomes a single-channel LL that plays the role of a lead. The rMZM is expected at the interface between 2-channel LL and single-channel LL ($x = 0$).

The transport physics of 2LL/LL junction is characterized by tunneling fixed points. Fig. 2 (c) - (e) depict three stable fixed points for different physical boundary conditions at the interface. (i) Disconnecting fixed point (DFP) signals the promotion of normal reflection process, where electrons will be perfectly reflected at the interface between 2LL and LL (Fig. 2 (c)). (ii) Pair-tunneling fixed point (PFP) characterizes the resonant Andreev reflection process [37], where electrons will pair up and tunnel through the interface without any backscattering, as shown in Fig. 2 (d). (iii) A_0 fixed point (A_0 FP) also signals normal reflection process of electrons from the LL lead, while on the 2LL side, electrons of channel-1 (channel-2) will pair up and be scattered together into channel-2 (channel-1) at the interface, as shown in Fig. 2 (e). This is essentially different from the case of DFP,

where electrons will be individually backscattered without any channel-switching. We notice that DFP and PFP have been previously discussed in a TSC/LL junction [38], while A_0 FP is a new fixed point in our system.

With the “delayed evaluation of boundary condition” (DEBC) method [39, 40], we verified the existence of all three fixed points (DFP, PFP, and A_0 FP) and evaluate the scaling dimensions of perturbation terms at each fixed point. A brief introduction of this method and details of fixed point information can be found in the supplementary materials [27]. The complete phase diagram is mapped out in Fig. 2 (b) for $K_- < 1$. In the strongly attractive regime ($K_+ < 1 - 2K_0$), PFP is stable and promotes the Andreev reflection process. In the strongly repulsive limit ($K_+ > 4 - 2K_0$), both DFP and A_0 FP are stable, and the tunneling conductance is suppressed.

A realistic system is most likely to fall into the weakly interacting regime ($K_0, K_+ \approx 1$) with both stable PFP and A_0 FP. In a transport measurement, one expects a zero-bias conductance peak at PFP, while a vanishing conductance at A_0 FP. The co-existence of two stable fixed points suggests the emergence of an intermediate unstable fixed point which characterizes the transition between PFP and A_0 FP. This novel phase transition is intriguing, which is definitely worthy to be explored in future works. At last, the role of rMZM is explored by mapping out a Majorana-free phase diagram where we quench pair-hopping interaction g at $x > 0$. In this case, we find a completely different phase diagram with more exotic phases [27]. Especially, the system falls into A_0 FP near $K_{0,+} \approx 1$, while PFP only shows up in the strongly attractive regime. Therefore, the appearance of weakly interacting PFP in Fig. 2 (b) is a direct consequence of

rMZM, and serves as a transport evidence of rMZM.

Discussion - In summary, we have proposed that magnetic-flux insertion drives DSM nanowire into a 1D crystalline-symmetry-protected semimetal, which serves as an ideal platform to realize Majorana physics without long-range superconductivity. In particular, crystalline symmetry forbids inter-channel single-particle tunneling, and thus guarantees the stability of Majorana physics. We notice that DSM nanowire of Cd_3As_2 has been successfully fabricated [41, 42], while these nanowires have been grown along [112] direction, so that C_4 rotation symmetry is explicitly broken and fails to support rMZM. Other promising candidate materials include heterostructures of Kondo materials [43], where a correlated DSM phase protected by C_4 symmetry is found. Finally, we emphasize once again that our theory is general and not limited to the DSM nanowires. The classification of 2D point groups in the supplementary materials will inspire more future efforts into realizing symmetry-protected Majoranas in number conserving systems.

Acknowledgement - The authors are indebted to Meng Cheng for valuable suggestions. R.-X.Z would like to thank Jian-Xiao Zhang, Jiabin Yu and Jiahua Gu for helpful discussions, and particularly Lun-Hui Hu for collaboration on a closely related project. C.-X. L. and R.-X.Z acknowledge support from Office of Naval Research (Grant No. N00014-15-1-2675).

-
- [1] C. Nayak, S. H. Simon, A. Stern, M. Freedman, and S. D. Sarma, *Reviews of Modern Physics* **80**, 1083 (2008).
- [2] D. C. Tsui, H. L. Stormer, and A. C. Gossard, *Physical Review Letters* **48**, 1559 (1982).
- [3] G. Moore and N. Read, *Nuclear Physics B* **360**, 362 (1991).
- [4] A. Y. Kitaev, *Annals of Physics* **303**, 2 (2003).
- [5] N. Read and D. Green, *Physical Review B* **61**, 10267 (2000).
- [6] D. A. Ivanov, *Physical Review Letters* **86**, 268 (2001).
- [7] A. Y. Kitaev, *Physics-Uspekhi* **44**, 131 (2001).
- [8] J. Alicea, *Reports on Progress in Physics* **75**, 076501 (2012).
- [9] R. M. Lutchyn, J. D. Sau, and S. D. Sarma, *Physical review letters* **105**, 077001 (2010).
- [10] Y. Oreg, G. Refael, and F. von Oppen, *Physical review letters* **105**, 177002 (2010).
- [11] V. Mourik, K. Zuo, S. M. Frolov, S. Plissard, E. Bakkers, and L. P. Kouwenhoven, *Science* **336**, 1003 (2012).
- [12] A. Das, Y. Ronen, Y. Most, Y. Oreg, M. Heiblum, and H. Shtrikman, *Nature Physics* **8**, 887 (2012).
- [13] S. Nadj-Perge, I. K. Drozdov, J. Li, H. Chen, S. Jeon, J. Seo, A. H. MacDonald, B. A. Bernevig, and A. Yazdani, *Science* **346**, 602 (2014).
- [14] H. Zhang, C.-X. Liu, S. Gazibegovic, D. Xu, J. A. Logan, G. Wang, N. van Loo, J. D. Bommer, M. W. de Moor, D. Car, et al., *arXiv preprint arXiv:1710.10701* (2017).
- [15] L. Fidkowski, R. M. Lutchyn, C. Nayak, and M. P. Fisher, *Physical Review B* **84**, 195436 (2011).
- [16] M. Cheng and H.-H. Tu, *Physical Review B* **84**, 094503 (2011).
- [17] J. D. Sau, B. Halperin, K. Flensberg, and S. D. Sarma, *Physical Review B* **84**, 144509 (2011).
- [18] C. V. Kraus, M. Dalmonte, M. A. Baranov, A. M. Läuchli, and P. Zoller, *Physical review letters* **111**, 173004 (2013).
- [19] G. Ortiz, J. Dukelsky, E. Cobanera, C. Esebbag, and C. Beenakker, *Physical review letters* **113**, 267002 (2014).
- [20] J. Klinovaja and D. Loss, *Physical review letters* **112**, 246403 (2014).
- [21] F. Iemini, L. Mazza, D. Rossini, R. Fazio, and S. Diehl, *Physical review letters* **115**, 156402 (2015).
- [22] N. Lang and H. P. Büchler, *Physical Review B* **92**, 041118 (2015).
- [23] C. Chen, W. Yan, C. Ting, Y. Chen, and F. Burnell, *arXiv preprint arXiv:1701.01794* (2017).
- [24] F. Iemini, L. Mazza, L. Fallani, P. Zoller, R. Fazio, and M. Dalmonte, *Physical Review Letters* **118**, 200404 (2017).
- [25] Z. Wang, Y. Sun, X.-Q. Chen, C. Franchini, G. Xu, H. Weng, X. Dai, and Z. Fang, *Physical Review B* **85**, 195320 (2012).
- [26] Z. Wang, H. Weng, Q. Wu, X. Dai, and Z. Fang, *Physical Review B* **88**, 125427 (2013).
- [27] See Supplementary Materials at XX for a solution of Dirac semimetal in cylindrical coordinates, the magnetic field dependence, a microscopic derivation of pair-hopping interaction g , an estimation of the magnitude of g , a discussion about Klein factors and the Majorana solution at Luther-Emery point, a discussion of the emergent Z_M fermion parity from a Z_N symmetry, a generalization from C_4 symmetry to the 2D point groups, a detailed calculation of single electron tunneling amplitude, an introduction of DEBC method and a detailed discussion about the 2LL/LL junction phase diagram, which contains [44–53].
- [28] K.-I. Imura and Y. Takane, *Physical Review B* **84**, 245415 (2011).
- [29] In the limit $R \rightarrow \infty$, the energy gap in both spin sectors approaches zero and DSM nanowire evolves into a bulk DSM sample with two bulk Dirac points connected by Fermi arc states.
- [30] G. Rosenberg, H.-M. Guo, and M. Franz, *Physical Review B* **82**, 041104 (2010).
- [31] The nanowire configuration is modeled by taking periodic (open) boundary condition along the z (x and y) direction. Realistic parameters of Cd_2As_3 are applied in the calculation, and the cross section in the x - y plane is chosen to be a 16×16 square.
- [32] Notice that the effective $k \cdot p$ Hamiltonian in Eq. 9 has the full-rotation $O(2)$ symmetry, since we focused on the continuum limit and dropped higher order terms. However, when we consider interaction effects, it is important to distinguish this artificial $O(2)$ symmetry from the realistic C_4 symmetry. This is because $O(2)$ is a stronger symmetry and also imposes a stronger constraint to interaction terms. In particular, the pair-hopping term g that leads to Majorana physics transfers angular momentum by $\Delta J_{tot} = 4$. As a result, pair-hopping interaction only preserves C_4 symmetry, but explicitly breaks $O(2)$ symmetry.
- [33] T. Giamarchi, *Quantum physics in one dimension*, Vol. 121 (Oxford university press, 2004).

- [34] E. Fradkin, Field theories of condensed matter physics (Cambridge University Press, 2013).
- [35] D. J. Clarke, J. Alicea, and K. Shtengel, *Nature Communications* **4**, 1348 (2013).
- [36] A. Keselman and E. Berg, *Physical Review B* **91**, 235309 (2015).
- [37] K. T. Law, P. A. Lee, and T. K. Ng, *Physical review letters* **103**, 237001 (2009).
- [38] L. Fidkowski, J. Alicea, N. H. Lindner, R. M. Lutchyn, and M. P. Fisher, *Physical Review B* **85**, 245121 (2012).
- [39] M. Oshikawa, C. Chamon, and I. Affleck, *Journal of Statistical Mechanics: Theory and Experiment* **2006**, P02008 (2006).
- [40] C.-Y. Hou, A. Rahmani, A. E. Feiguin, and C. Chamon, *Physical Review B* **86**, 075451 (2012).
- [41] C.-Z. Li, L.-X. Wang, H. Liu, J. Wang, Z.-M. Liao, and D.-P. Yu, *Nature communications* **6** (2015).
- [42] L.-X. Wang, C.-Z. Li, D.-P. Yu, and Z.-M. Liao, *Nature communications* **7** (2016).
- [43] S. Ok, M. Legner, T. Neupert, and A. M. Cook, *arXiv preprint arXiv:1703.03804* (2017).
- [44] C. Kane, R. Mukhopadhyay, and T. Lubensky, *Physical review letters* **88**, 036401 (2002).
- [45] J. C. Teo and C. Kane, *Physical Review B* **89**, 085101 (2014).
- [46] T. Neupert, C. Chamon, C. Mudry, and R. Thomale, *Physical Review B* **90**, 205101 (2014).
- [47] E. Sagi and Y. Oreg, *Physical Review B* **90**, 201102 (2014).
- [48] J. Klinovaja and Y. Tserkovnyak, *Physical Review B* **90**, 115426 (2014).
- [49] B. Bellazzini, M. Mintchev, and P. Sorba, *Journal of Physics A: Mathematical and Theoretical* **40**, 2485 (2007).
- [50] B. Bellazzini, M. Burrello, M. Mintchev, and P. Sorba, *arXiv preprint arXiv:0801.2852* (2008).
- [51] B. Bellazzini, M. Mintchev, and P. Sorba, *Physical Review B* **80**, 245441 (2009).
- [52] A. Agarwal, S. Das, S. Rao, and D. Sen, *Physical review letters* **103**, 026401 (2009).
- [53] J.-P. Jay-Gerin, M. Aubin, and L. Caron, *Solid State Communications* **21**, 771 (1977).

Supplementary Materials for “Crystalline symmetry protected Majorana mode in number-conserving Dirac semi-metal nanowires”

APPENDIX A. DIRAC SEMIMETAL IN CYLINDRICAL COORDINATES

In this appendix, we will follow Ref. [28] to derive the low-energy theory of DSM nanowire in a cylindrical geometry. A typical Hamiltonian for Dirac semimetals (such as Na_3Bi and Cd_3As_2) is given by [25, 26]

$$H_{Dirac} = \begin{pmatrix} H_{\uparrow} & 0 \\ 0 & H_{\downarrow} \end{pmatrix} = \begin{pmatrix} M(k) & Ak_- & 0 & 0 \\ Ak_+ & -M(k) & 0 & 0 \\ 0 & 0 & -M(k) & -Ak_- \\ 0 & 0 & -Ak_+ & M(k) \end{pmatrix}. \quad (9)$$

The basis functions are $|P, \frac{3}{2}\rangle, |S, \frac{1}{2}\rangle, |S, -\frac{1}{2}\rangle, |P, -\frac{3}{2}\rangle$. Here $M(k) = M_0 - M_1k_z^2 - M_2(k_x^2 + k_y^2)$ and $k_{\pm} = k_x \pm ik_y$, with $A > 0$ and $M_{0,1,2} > 0$. The bulk Dirac points are $k_z = \pm K_0 = \pm \sqrt{\frac{M_0}{M_1}}$. Notice that $H_{\downarrow}(M(k), A) = H_{\uparrow}(-M(k), -A)$ and we will focus on H_{\uparrow} in the following discussion. In cylindrical coordinate, $(x, y, z) \rightarrow (r, \theta, z)$ with

$$r = \sqrt{x^2 + y^2}, \quad \theta = \arctan \frac{y}{x}. \quad (10)$$

It is easy to show that

$$\begin{aligned} k_+ &= e^{i\theta}(k_r + ik_{\theta}) \\ k_- &= e^{-i\theta}(k_r - ik_{\theta}) \end{aligned} \quad (11)$$

with $k_r = -i\frac{\partial}{\partial r}$ and $k_{\theta} = -i\frac{1}{r}\frac{\partial}{\partial \theta}$. When the radius r is much larger than the lattice constant a with $r \gg a$, we also have $k_x^2 + k_y^2 = k_r^2 + k_{\theta}^2$. Then H_{\uparrow} can be separated into $H_{\uparrow,\perp}$ describing the physics normal to the surface and $H_{\uparrow,\parallel}$ describing the physics parallel to the surface. Let us consider the physics around some k_0 on the k_z axis, with $k_z = k_0 + \delta k_z$. For simplicity, we will use k_z to represent δk_z in the later discussion. We find that

$$H_{\uparrow,\perp} = \begin{pmatrix} N(k_0) - M_2k_r^2 & Ae^{-i\theta}k_r \\ Ae^{i\theta}k_r & -N(k_0) + M_2k_r^2 \end{pmatrix} \quad (12)$$

and

$$H_{\uparrow,\parallel} = \begin{pmatrix} -2M_1k_0k_z - M_1k_z^2 - M_2k_{\theta}^2 & -iAe^{-i\theta}k_{\theta} \\ iAe^{i\theta}k_{\theta} & 2M_1k_0k_z + M_1k_z^2 + M_2k_{\theta}^2 \end{pmatrix}. \quad (13)$$

Here $N(k_0) = M_0 - M_1 k_0^2$. The strategy here is to solve for eigenstate of $H_{\uparrow,\perp}$ with open boundary condition and use this result to project $H_{\uparrow,\parallel}$ to extract low-energy effective theory of the Dirac semimetal nanowire. Let us assume the radius of the nanowire is $R \gg a$, and the open boundary condition is $\psi_{\perp}(r = R) = 0$. Then a trial wavefunction of $H_{\uparrow,\perp}$ should take the form

$$\psi_{\perp,\lambda}(r) \sim e^{\lambda(r-R)} \begin{pmatrix} C \\ D e^{i\theta} \end{pmatrix} \quad (14)$$

Then the energy eigenstate with energy E can be shown to take the form

$$\psi_{\perp,\lambda}(E, r) \sim e^{\lambda(r-R)} \begin{pmatrix} E + m(\lambda) \\ -i\lambda A e^{i\theta} \end{pmatrix} \quad (15)$$

where $m(\lambda) = N_0 + M_2 \lambda^2$. On the other hand, eigen-equation now becomes

$$\det \begin{pmatrix} m(\lambda) - E & -iAe^{-i\theta}\lambda \\ -iAe^{i\theta}\lambda & -m(\lambda) - E \end{pmatrix} = 0 \quad (16)$$

λ_{\pm} are the two positive λ solutions of the above equation, and they satisfy

$$\lambda_+ \lambda_- = \sqrt{\frac{N_0^2 - E^2}{M_2^2}} \quad (17)$$

Notice that these solutions only exist when $|E| < |N_0|$. This implies that the surface state solutions are in-gap states which live at $-k_0 < k_z < k_0$. The wavefunction now can be written as a linear superposition of λ_+ and λ_- eigenstates,

$$\psi_{\perp}(E, r) = c_+ e^{\lambda_+(r-R)} \psi_{\perp,\lambda_+} + c_- e^{\lambda_-(r-R)} \psi_{\perp,\lambda_-} \quad (18)$$

The boundary condition at $r = R$ indicates that

$$\det \begin{pmatrix} m(\lambda_+) + E & m(\lambda_-) + E \\ -iAe^{i\theta}\lambda_+ & -iAe^{i\theta}\lambda_- \end{pmatrix} = 0 \quad (19)$$

After some calculations, we find that

$$E(E + N_0) = 0 \quad (20)$$

For $|E| < |N_0|$, the only solution is

$$\begin{aligned} E &= 0 \\ m(\lambda) &= \pm A\lambda \end{aligned} \quad (21)$$

Together with the definition of $m(\lambda)$, λ_{\pm} must satisfy

$$M_2 \lambda^2 \mp A\lambda + N_0 = 0 \quad (22)$$

or equivalently

$$\begin{aligned} \lambda_+ + \lambda_- &= \pm \frac{A}{2M_2} \\ \lambda_+ \lambda_- &= \frac{N_0}{M_2} \end{aligned} \quad (23)$$

Since $\lambda_{\pm} > 0$, we have $m(\lambda) = A\lambda$ and $N_0 > 0$, which implies $|k_0| < \frac{M_0}{M_1} = K_0$. Therefore, this in-gap surface states only exists between two bulk Dirac points, and are identified as the Fermi arc states connecting the bulk Dirac points. The surface state wavefunction now takes the form

$$\psi_{\perp}(E, r, \theta) = f(\lambda_{\pm}, r) \begin{pmatrix} 1 \\ -i e^{i\theta} \end{pmatrix} \quad (24)$$

Now let us obtain the projected low energy theory of $H_{\uparrow,\parallel}$, and we find that

$$\begin{aligned} H_{\uparrow,eff} &= \psi_{\perp}^{\dagger} H_{\uparrow,\parallel} \psi_{\perp} \\ &= -\frac{A}{r} \left(-i \frac{\partial}{\partial \theta} + \frac{1}{2} \right) + \frac{M_2}{r^2} \left(1 - 2i \frac{\partial}{\partial \theta} \right) \end{aligned} \quad (25)$$

With periodic boundary condition along $\hat{\theta}$ direction, k_θ is a good quantum number and $-i\partial_\theta$ operator takes integer values $m = 0, 1, 2, 3, \dots$. It is easy to see that the lowest energy state locates at $r = R$, and when $R \gg a$, the second term in $H_{\uparrow,eff}$ can be ignored. We find that

$$E_{\uparrow,eff} = -\frac{A}{R}(m + \frac{1}{2}). \quad (26)$$

As for the spin-down part, since $H_\downarrow(M(k), A) = H_\uparrow(-M(k), -A)$, it is easy to see that

$$E_{\downarrow,eff} = \frac{A}{R}(m + \frac{1}{2}). \quad (27)$$

It is easy to see that the energy spectrum is gapped because of the π Berry phase which gives rise to a $\frac{A}{R}$ energy gap.

To remove the Berry phase effect, we apply a magnetic field, which must be carefully aligned along the nanowire to preserve the rotation symmetry of the system. Assume the flux is $\Psi = l\Psi_0$ with $\Psi_0 = \frac{h}{e}$ being the flux quantum, the energy spectrum is modified to

$$\begin{aligned} E_{\uparrow,eff} &= -\frac{A}{R}(m + \frac{1}{2} - l) \\ E_{\downarrow,eff} &= \frac{A}{R}(m + \frac{1}{2} - l) \end{aligned} \quad (28)$$

Therefore, inserting magnetic flux shifts $E_{\uparrow,eff}$ by $\frac{lA}{R}$ and $E_{\downarrow,eff}$ by $-\frac{lA}{R}$. When $l > \frac{1}{2}$, we find that $|m = 0, \uparrow\rangle$ ($m = 0$ state in the spin up sector) and $|m = 0, \downarrow\rangle$ form gapless inverted band structure, leading to semimetallic dispersions.

As a result of Eq. 24, a state labeled with m can be written as

$$\begin{aligned} |m, \uparrow\rangle &\sim e^{im\theta} |\psi_\perp, \uparrow\rangle = e^{im\theta} (|\frac{3}{2}\rangle - ie^{i\theta} |\frac{1}{2}\rangle) \\ |m, \downarrow\rangle &\sim e^{im\theta} |\psi_\perp, \downarrow\rangle = e^{im\theta} (|-\frac{1}{2}\rangle - ie^{i\theta} |-\frac{3}{2}\rangle) \end{aligned} \quad (29)$$

where we have ignored its r and k_z dependence. Therefore, even with the same m value, the spin-up state and the spin-down state have different angular momentum. Their angular momentum can be read out when we apply a rotation operator $C_\theta = e^{iJ\theta}$, and we find that

$$\begin{aligned} C_\theta |m, \uparrow\rangle &= e^{i(m+\frac{3}{2})\theta} |m, \uparrow\rangle \quad \text{with } J = m + \frac{3}{2} \\ C_\theta |m, \downarrow\rangle &= e^{i(m-\frac{1}{2})\theta} |m, \downarrow\rangle \quad \text{with } J = m - \frac{1}{2} \end{aligned} \quad (30)$$

Therefore, $|m = 0, \uparrow\rangle$ carries angular momentum $J = \frac{3}{2}$ while $|m = 0, \downarrow\rangle$ carries angular momentum $J = -\frac{1}{2}$. These two states belong to different representations of rotation group, and the crossing between them is protected.

In our discussion, we create only one pair of Dirac points with flux number $\frac{1}{2} < l < \frac{3}{2}$. In general, one can keep increasing flux to create more 1D Dirac points, realizing an N-channel LL ($N > 2$) system. Such N-channel LL could be a potential realization of coupled wire system, whose interaction effects have been widely discussed [44–48].

In Fig. 3, we numerically calculate the magnetic field for inducing 2π magnetic flux in a nanowire with a radius r . For the existing nanowire setup of Cd_3As_2 [42] with a diameter of around 100 nm, the magnetic field for 2π -flux is around 0.8T.

APPENDIX B. MICROSCOPIC ORIGIN OF PAIR-HOPPING INTERACTION

In this section, we will discuss the microscopic origin of pair-hopping interaction g . Let us recall that the low-energy physics originates from the following channels:

$$\begin{aligned} \text{Channel 1: } |m = 0, \downarrow\rangle &\sim |-\frac{1}{2}\rangle - ie^{i\theta} |-\frac{3}{2}\rangle \\ \text{Channel 2: } |m = 0, \uparrow\rangle &\sim |\frac{3}{2}\rangle - ie^{i\theta} |\frac{1}{2}\rangle \end{aligned} \quad (31)$$

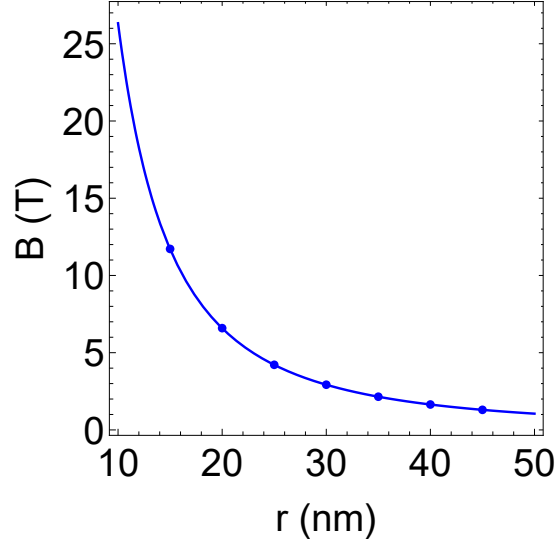


FIG. 3. The magnetic field for inducing 2π flux in a nanowire with a radius r .

We can expand the angular momentum bases with the bases of spin and atomic orbitals as follows,

$$\begin{aligned}
\left|\frac{3}{2}\right\rangle &= \beta_1 |p_+, \uparrow\rangle + \dots \\
\left|\frac{1}{2}\right\rangle &= \alpha_2 |s, \uparrow\rangle + \beta_2 |p_+, \downarrow\rangle + \dots \\
\left|-\frac{1}{2}\right\rangle &= \alpha_3 |s, \downarrow\rangle + \beta_3 |p_-, \uparrow\rangle + \dots \\
\left|-\frac{3}{2}\right\rangle &= \beta_4 |p_-, \downarrow\rangle + \dots
\end{aligned} \tag{32}$$

where α_i and β_i are coefficients that depend on material details. Now, we will start from the pair-hopping interaction g and trace back its microscopic origin in the atomic orbital bases:

$$\begin{aligned}
H_1 &= g \int dx \int_0^{2\pi} R d\theta \psi_{2,R}^\dagger \psi_{2L}^\dagger \psi_{1,R} \psi_{1,L} \\
&= g \int dx \int_0^{2\pi} R d\theta (c_{\frac{3}{2},R}^\dagger + ie^{-i\theta} c_{\frac{1}{2},R}^\dagger)(c_{\frac{3}{2},L}^\dagger + ie^{-i\theta} c_{\frac{1}{2},L}^\dagger)(c_{-\frac{1}{2},R} - ie^{i\theta} c_{-\frac{3}{2},R}^\dagger)(c_{-\frac{1}{2},L} - ie^{i\theta} c_{-\frac{3}{2},L}^\dagger) \\
&= g \int_0^{2\pi} R d\theta [(V_{3311} + V_{1133} + V_{3113} + V_{1331} + V_{3131} + V_{1313}) + e^{-i\theta} V_{-1} + e^{i\theta} V_1 + e^{-2i\theta} V_{-2} + e^{2i\theta} V_2] \tag{33}
\end{aligned}$$

where we have defined

$$V_{ijkl} = \int dx \psi_{\frac{i}{2},R}^\dagger \psi_{\frac{j}{2},L}^\dagger \psi_{-\frac{k}{2},R} \psi_{-\frac{l}{2},L} \tag{34}$$

The explicit form of $V_{\pm 1(2)}$ are not important to our analysis, since these terms will vanish under the integral of angular variable θ :

$$\int_0^{2\pi} e^{in\theta} d\theta = 2\pi \delta_{n,0}, \quad \forall n \in \mathbb{Z} \tag{35}$$

Therefore,

$$H_1 = 2\pi g \int dx (V_{3311} + V_{1133} + V_{3113} + V_{1331} + V_{3131} + V_{1313}) \tag{36}$$

Let us take V_{3113} as an example. In the momentum space representation,

$$\begin{aligned}
V_{3113} &= \sum_{k,k',q} \beta_1^* \beta_4 c_{p_+, \uparrow, k}^\dagger (\alpha_2^* c_{s, \uparrow, k'}^\dagger + \beta_2^* c_{p_+, \downarrow, k'}^\dagger) (\alpha_3 c_{s, \downarrow, k'+q} + \beta_3 c_{p_-, \uparrow, k'+q}) c_{p_-, \downarrow, k-q} \\
&= \beta_1^* \alpha_2^* \alpha_3 \beta_4 \sum_q \left(\sum_k c_{p_+, \uparrow, k}^\dagger c_{p_-, \downarrow, k-q} \right) \left(\sum_{k'} c_{s, \uparrow, k'}^\dagger c_{s, \downarrow, k'+q} \right) \\
&\quad + \beta_1^* \beta_2^* \beta_3 \beta_4 \sum_q \left(\sum_k c_{p_+, \uparrow, k}^\dagger c_{p_-, \downarrow, k-q} \right) \left(\sum_{k'} c_{p_+, \downarrow, k'}^\dagger c_{p_-, \uparrow, k'+q} \right) + \dots \\
&= \beta_1^* \alpha_2^* \alpha_3 \beta_4 \sum_q S_{p, \frac{3}{2}}^+(q) S_{s, \frac{1}{2}}^+(-q) + \beta_1^* \beta_2^* \beta_3 \beta_4 \sum_q S_{p, \frac{3}{2}}^+(q) S_{p, \frac{3}{2}}^-(-q) + \dots
\end{aligned} \tag{37}$$

Here we have defined the spin operators as

$$\begin{aligned}
S_{p, \frac{3}{2}}^i(q) &= \sum_k (c_{p_+, \uparrow, k+q}^\dagger, c_{p_-, \downarrow, k+q}^\dagger) \tau^i \begin{pmatrix} c_{p_+, \uparrow, k} \\ c_{p_-, \downarrow, k} \end{pmatrix} \\
S_{p, \frac{1}{2}}^i(q) &= \sum_k (c_{p_-, \uparrow, k+q}^\dagger, c_{p_+, \downarrow, k+q}^\dagger) \tau^i \begin{pmatrix} c_{p_-, \uparrow, k} \\ c_{p_+, \downarrow, k} \end{pmatrix} \\
S_{s, \frac{1}{2}}^i(q) &= \sum_k (c_{s, \uparrow, k+q}^\dagger, c_{s, \downarrow, k+q}^\dagger) \tau^i \begin{pmatrix} c_{s, \uparrow, k} \\ c_{s, \downarrow, k} \end{pmatrix}
\end{aligned} \tag{38}$$

where $\tau^{i=x,y,z}$ is the Pauli matrix. The spin ladder operators are defined as

$$S_{\alpha, J}^\pm = S_{\alpha, J}^x \pm i S_{\alpha, J}^y \tag{39}$$

Physically, the first term in V_{3113} flips two spin simultaneously, which could originate from the combinational effects of Coulomb interaction and spin-orbit coupling. The second term is the conventional multi-orbital Coulomb exchange interaction.

APPENDIX C. EXPRESSIONS OF K_+ AND K_-

In this section, we consider the renormalization effects of the following density-density interactions to the Luttinger parameters K_+ and K_- .

$$V_{density} = g_3 \sum_{s=1,2} \rho_{s,L} \rho_{s,R} + g_4 \sum_{s \neq s' \in \{1,2\}} \rho_{s,L} \rho_{s',R} + g_5 \sum_{s=1,2} (\rho_{s,L}^2 + \rho_{s,R}^2) \tag{40}$$

Here, g_3 and g_4 denote intra-channel and inter-channel interactions, respectively. In the bosonization language, density operators are defined as

$$\begin{aligned}
\rho_{s,L} &= \frac{1}{2\sqrt{\pi}} \partial_x (\phi_s + \theta_s) \\
\rho_{s,R} &= \frac{1}{2\sqrt{\pi}} \partial_x (\phi_s - \theta_s)
\end{aligned} \tag{41}$$

Each term of $V_{density}$ can be bosonized into

$$\begin{aligned}
g_3 \sum_{s=1,2} \rho_{s,L} \rho_{s,R} &= \frac{g_3}{4\pi} [(\partial_x \phi_1)^2 - (\partial_x \theta_1)^2 + (\partial_x \phi_2)^2 - (\partial_x \theta_2)^2] \\
&= \frac{g_3}{4\pi} [(\partial_x \phi_+)^2 - (\partial_x \theta_+)^2 + (\partial_x \phi_-)^2 - (\partial_x \theta_-)^2]
\end{aligned} \tag{42}$$

$$\begin{aligned}
g_4 \sum_{s \neq s' \in \{1,2\}} \rho_{s,L} \rho_{s',R} &= \frac{g_4}{2\pi} [(\partial_x \phi_1)(\partial_x \phi_2) - (\partial_x \theta_1)(\partial_x \theta_2)] \\
&= \frac{g_4}{4\pi} [(\partial_x \phi_+)^2 - (\partial_x \theta_+)^2 - (\partial_x \phi_-)^2 + (\partial_x \theta_-)^2]
\end{aligned} \tag{43}$$

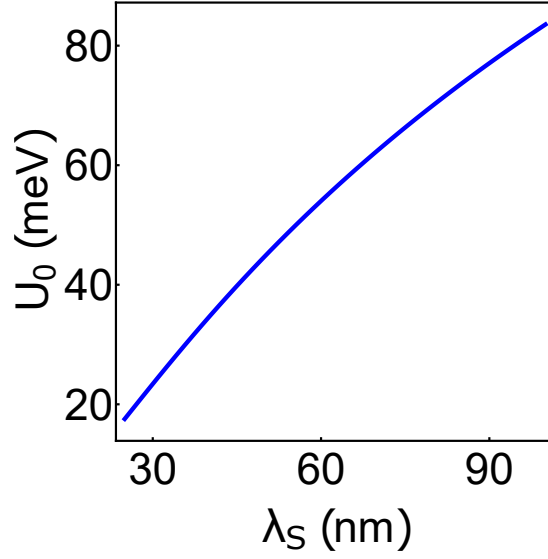


FIG. 4. The dependence of interaction strength U_0 on the screening length λ_s .

$$\begin{aligned}
g_5 \sum_{s=1,2} (\rho_{s,L}^2 + \rho_{s,R}^2) &= \frac{g_5}{2\pi} (\partial_x \phi_1)^2 + (\partial_x \theta_1)^2 + (\partial_x \phi_2)^2 + (\partial_x \theta_2)^2 \\
&= \frac{g_5}{2\pi} [(\partial_x \phi_+)^2 + (\partial_x \theta_+)^2 + (\partial_x \phi_-)^2 + (\partial_x \theta_-)^2]
\end{aligned} \tag{44}$$

It is then straightforward to arrive at

$$\begin{aligned}
K_+ &= \sqrt{\frac{v_f + \frac{1}{2\pi}(2g_5 + g_3 + g_4)}{v_f + \frac{1}{2\pi}(2g_5 - g_3 - g_4)}} \\
K_- &= \sqrt{\frac{v_f + \frac{1}{2\pi}(2g_5 + g_3 - g_4)}{v_f + \frac{1}{2\pi}(2g_5 - g_3 + g_4)}}
\end{aligned} \tag{45}$$

To make pair-hopping interaction g relevant, we require that $K_- < 1$, which is equivalent to $g_3 < g_4$.

APPENDIX D. ESTIMATION OF g

In this section, we give a rough estimation of the magnitude of g . Our starting point is the standard Coulomb interaction,

$$U_C = \sum_{i,j \in \{1,2\}} \int d^3\mathbf{r} d^3\mathbf{r}' \rho_i(\mathbf{r}) V(\mathbf{r} - \mathbf{r}') \rho_j(\mathbf{r}') \tag{46}$$

where i and j are the channel index. In the cylindrical geometry, $\mathbf{r} = (r \cos \theta, r \sin \theta, x)$. The screened Coulomb potential is defined as

$$V(\mathbf{r}) = \frac{e^2}{4\pi\epsilon_0\epsilon} \frac{1}{|\mathbf{r}|} e^{-|\mathbf{r}|/\lambda_s} \tag{47}$$

where λ_s is the screening length to be determined. A general electron operator in the cylindrical geometry can be written as follows:

$$c_i^\dagger(\mathbf{r}) = \frac{1}{L} f(r, \theta) \sum_k e^{ikx} c_i^\dagger(k) \tag{48}$$

where $f(r, \theta)$ is the radial and angular part of the wavefunction. k is the momentum defined in the x direction (along the nanowire). The density operator is then defined as

$$\rho_i(\mathbf{r}) = \frac{1}{L} |f(r, \theta)|^2 \rho_i(x) = \frac{1}{L} |f(r, \theta)|^2 \sum_q \rho_i(q) e^{iqx}. \quad (49)$$

Since we are only interested in the Fermi-arc states which are exponentially localized along the radial direction, we assume $r \ll x$ in the long nanowire limit, and find that

$$|\mathbf{r} - \mathbf{r}'| = \sqrt{(r \cos \theta - r' \cos \theta')^2 + (r \sin \theta - r' \sin \theta')^2 + (x - x')^2} \approx |x - x'|. \quad (50)$$

Back to U_C , we find that

$$\begin{aligned} U_C &\approx \frac{1}{L^2} \sum_{i,j} \left(\int r dr d\theta |f(r, \theta)|^2 \right) \left(\int r' dr' d\theta' |f(r', \theta')|^2 \right) \int dx \int dx' \sum_{q,q'} \rho_i(q) \rho_j(q') e^{iqx+iq'x'} V(x-x') \\ &= \frac{1}{L^2} \sum_{i,j} \int dx \int dx' \sum_{q,q'} \rho_i(q) \rho_j(q') e^{iqx+iq'x'} V(x-x') \\ &= \frac{1}{L^2} \sum_{i,j} \int dx \int d\tilde{x} \sum_{q,q'} \rho_i(q) \rho_j(q') e^{i(q+q')x} V(\tilde{x}) e^{-iq'\tilde{x}} \\ &= \sum_{i,j} \int d\tilde{x} V(\tilde{x}) \sum_q \rho_i(q) \rho_j(-q) \\ &= \sum_{i,j} \int d\tilde{x} V(\tilde{x}) \int dx \rho_i(x) \rho_j(x). \end{aligned} \quad (51)$$

Here we have applied the long wave-length limit: $\lim_{q' \rightarrow 0} e^{-iq'\tilde{x}} = 1$. Therefore, the four fermion contact interaction in the Luttinger liquid theory corresponds to the zero-momentum component of Coulomb interaction. In other words, the following expression will give us a rough estimation of the interaction strength in our system,

$$U_0 = 2 \int_{x>0} dx \frac{e^2}{4\pi\epsilon_0\epsilon} \frac{1}{x} e^{-x/\lambda_s} \approx \int_{l_B}^{\lambda_s} dx \frac{e^2}{2\pi\epsilon_0\epsilon} \frac{1}{x} = \frac{e^2}{2\pi\epsilon_0\epsilon} \ln\left(\frac{\lambda_s}{l_B}\right), \quad (52)$$

where l_B is the magnetic length. As we have demonstrated in Appendix B, for $r = 50$ nm, the magnetic field for inducing 2π flux is around $1T$. This gives rise to a magnetic length of around 25 nm. For Cd_3As_2 , the static dielectric constant measured is $\epsilon \approx 36$ [53]. An accurate estimate for the screening length λ_s is difficult in our nanowire system. Thus, we take λ_s ranging from 10 to 100 nm and numerically plot the dependence of U_0 on the screening length in Fig. 4. We find that U_0 will increase with λ_s and is typically around dozens of meV.

APPENDIX E. REFERMIONIZATION AND KLEIN FACTORS

Introducing Klein factors is necessary to guarantee the anti-commutation relations of fermionic operators before and after the bosonization process, especially in a multiple-channel Luttinger liquid system. Meanwhile, Klein factors act as ladder operators in the Fock space of fermions. In this section, we present a detailed discussion of the role of Klein factors in our theory [16]. In particular, we focus on the Luther-Emery point when the model is exactly solvable. Recall that the standard Abelian bosonization takes the form:

$$\psi_{s,R} = \frac{\xi_{s,R}}{\sqrt{2\pi a_0}} e^{i\sqrt{\pi}(\phi_s - \theta_s)}, \quad \psi_{s,L} = \frac{\xi_{s,L}}{\sqrt{2\pi a_0}} e^{-i\sqrt{\pi}(\phi_s + \theta_s)}, \quad (53)$$

where a_0 is the short-distance cut-off. Klein factors $\xi_{l,R/L}$ satisfy the following relations,

$$\begin{aligned} [N_{s,h}, \xi_{s',h'}^\dagger] &= \xi_{s,h}^\dagger \delta_{h,h'} \delta_{s,s'}, & [N_{s,h}, \xi_{s',h'}] &= -\xi_{s,h} \delta_{h,h'} \delta_{s,s'}, \\ \{\xi_{s,h}, \xi_{s',h'}\} &= 0, & \{\xi_{s,h}, \xi_{s',h'}^\dagger\} &= 2\delta_{s,s'} \delta_{h,h'}, & \xi_{s,h} \xi_{s,h}^\dagger &= 1. \end{aligned} \quad (54)$$

Here $N_{s,h}$ is the number operators of fermions with channel index $s = 1, 2$ and chirality $h = R/L$. At the Luther-Emery point ($K_- = \frac{1}{2}$), we could map the pair-hopping interaction g into a spinless p-wave pairing term via refermionization

process:

$$\begin{array}{ccc}
\psi_{2,R}^\dagger \psi_{2,L}^\dagger \psi_{1,R} \psi_{1,L} & \xrightarrow{K_- = \frac{1}{2}} & \tilde{\psi}_R \tilde{\psi}_L \\
\downarrow \text{Bosonization} & & \uparrow \text{Refermionization} \\
\xi_{2,R}^\dagger \xi_{2,L}^\dagger \xi_{1,R} \xi_{1,L} e^{i2\sqrt{2}\pi\theta_-} & \xrightarrow{\text{Field rescaling}} & F_R F_L e^{i2\sqrt{\pi}\bar{\theta}}
\end{array} \tag{55}$$

As a result, we start from H_- with $K_- = \frac{1}{2}$ and arrive at the following Hamiltonian that turns out to be the Kitaev model:

$$H_- = iv \int dx (\tilde{\psi}_R^\dagger \partial_x \tilde{\psi}_R - \tilde{\psi}_L^\dagger \partial_x \tilde{\psi}_L) + im \int dx (\tilde{\psi}_R \tilde{\psi}_L + \tilde{\psi}_R^\dagger \tilde{\psi}_L^\dagger) \tag{56}$$

The new defined fermionic operators are

$$\tilde{\psi}_R = \frac{F_R}{\sqrt{2\pi a_0}} e^{i\sqrt{\pi}(\frac{\phi_-}{\sqrt{2}} - \sqrt{2}\theta_-)}, \quad \tilde{\psi}_L = \frac{F_L}{\sqrt{2\pi a_0}} e^{-i\sqrt{\pi}(\frac{\phi_-}{\sqrt{2}} + \sqrt{2}\theta_-)} \tag{57}$$

Following Ref. [16, 18], a natural choice for defining the new Klein factors would be

$$F_R = f_R \xi_{2,R}^\dagger \xi_{1,R}, \quad F_L = f_L \xi_{2,L}^\dagger \xi_{1,L}. \tag{58}$$

In the above definition, we have introduced an additional ‘‘Majorana’’ operator $f_{R/L}$ to guarantee the anti-commutation relation between F_R and F_L , which commutes with $N_{s,h}$ and thus acts trivially on the Fock space. One can easily check that

$$[N_{s,h}, F_{h'}] = (-1)^s F_h \delta_{h,h'}, \quad \text{where } s, s' \in \{1, 2\}, \quad h, h' \in \{R, L\}. \tag{59}$$

APPENDIX F. MAJORANA ZERO MODE AT LUTHER-EMERY POINT

We perform the Bogoliubov-de Gennes (BdG) transformation by defining the BdG basis

$$\tilde{\Psi} = \begin{pmatrix} \tilde{\psi}_R \\ \tilde{\psi}_L^\dagger \end{pmatrix} \tag{60}$$

Then H_- becomes a 1D massive Dirac Hamiltonian under the BdG basis:

$$H_- = \int dx \tilde{\Psi}^\dagger (iv \partial_x \sigma_z - m \sigma_y) \tilde{\Psi} \tag{61}$$

This Hamiltonian can be easily solved for boundary zero mode by imposing open boundary condition $\tilde{\Psi}(x < 0) = 0$, and we obtain a zero-mode solution that is exponentially localized at $x = 0$ [16]:

$$\alpha_1(x) = \sqrt{\frac{m}{v}} e^{-\frac{mx}{v}} \begin{pmatrix} 1 \\ 1 \end{pmatrix} \tilde{\Psi}(x) = \sqrt{\frac{m}{v}} e^{-\frac{mx}{v}} [\tilde{\psi}_R(x) + \tilde{\psi}_L^\dagger(x)] \tag{62}$$

In the bosonic language, we show in the main text that the open boundary condition requires

$$\phi_- = (2n_- - n_+) \sqrt{\frac{\pi}{2}}. \tag{63}$$

where $n_\pm \in \mathbb{Z}$. n_+ can be viewed as a c-number in our discussion, and we are free to take $n_+ = 0$ for simplicity. This bosonic boundary condition simply implies

$$\tilde{\psi}_R(x=0) = \tilde{\psi}_L(x=0) \tag{64}$$

This immediately leads to

$$\alpha_1 = \alpha_1^\dagger \tag{65}$$

at $x = 0$, and verified α_1 as a Majorana zero mode. At Luther-Emery point, it is clear that the bosonized form of α_1 (Eq. [6] in the main text) should inherit the Klein factor F_h from the bosonization formula of $\tilde{\psi}_h$.

APPENDIX G. SINGLE IMPURITY PROBLEM

In this section, we briefly discuss the stability of Majorana physics in the presence of C_4 -breaking disorders. For simplicity, we will focus on the case with a single impurity at $x = 0$. With such impurity, a left-moving electron in channel 1 can be either forward-scattered into a left-moving electron in channel 2 (denoted as T_1), or be backscattered into a right-moving electron in channel 2 (denoted as T_2). Since the scattering physics happens only at the impurity site $x = 0$, we are free to integrate out all bosonic fields except for the ones at $x = 0$. The system then reduces to a 0+1 dimensional field theory with,

$$\begin{aligned} T_1 &= t_1 \psi_{1,L}^\dagger(x=0) \psi_{2,L}(x=0) + h.c. \sim t_1 \cos \sqrt{2\pi}(\phi_- + \theta_-), \\ T_2 &= t_2 \psi_{1,L}^\dagger(x=0) \psi_{2,R}(x=0) + h.c. \sim t_2 \cos \sqrt{2\pi}(\phi_+ + \theta_-). \end{aligned} \quad (66)$$

The scaling dimensions of T_1 and T_2 are

$$\Delta(T_1) = \frac{1}{2}(K_- + \frac{1}{K_-}), \quad \Delta(T_2) = \frac{1}{2}(K_- + \frac{1}{K_+}). \quad (67)$$

Under renormalization group (RG) process, T_1 is always marginal or irrelevant. T_2 is irrelevant when $\Delta(T_2) > 1$, or equivalently

$$K_+ < \frac{1}{2 - K_-} \leq 1 \quad (68)$$

The second inequality is true when the pair-hopping interaction is relevant under RG ($K_- < 1$). Therefore, when Eq. 68 holds, C_4 -breaking impurity is irrelevant and the C_4 -protected Majorana physics is stable.

APPENDIX H. EMERGENT Z_M FERMION PARITY SYMMETRY FROM A Z_N SYMMETRY

In this section, we hope to establish the equivalence between a discrete Z_N symmetry with the fermion parity symmetry. As an example, we first start from the model of DSM nanowire with a C_4 rotation (Z_4) symmetry. According to the angular momentum representations, C_4 acts on the dual bosonic fields as,

$$C_4 \begin{pmatrix} \phi_+ \\ \phi_- \\ \theta_+ \\ \theta_- \end{pmatrix} = \begin{pmatrix} \phi_+ \\ \phi_- \\ \theta_+ - \frac{1}{2}\sqrt{\frac{\pi}{2}} \\ \theta_- + \sqrt{\frac{\pi}{2}} \end{pmatrix} \quad (69)$$

Thus, C_4 symmetry also interchanges $|\theta_- = \pm \frac{1}{2}\sqrt{\frac{\pi}{2}}\rangle$, which indicates that the degenerate ground states $|\pm\rangle$ are also eigen-states of C_4 symmetry operator. This proves the equivalence between C_4 symmetry and Z_2 parity in the low-energy sector.

Now let us consider a two-channel 1D system with a Z_N symmetry. The fermionic operators of different channels belong to distinct representations of the Z_N symmetry,

$$\begin{aligned} Z_N \psi_{1,L/R} Z_N^{-1} &= e^{i\frac{2\pi}{N}J} \psi_{1,L/R} \\ Z_N \psi_{2,L/R} Z_N^{-1} &= e^{i\frac{2\pi}{N}(J+k)} \psi_{2,L/R} \end{aligned} \quad (70)$$

where $0 \leq J < N$, $0 < k < N$ and $J, k \in \mathbb{Z}$. A general multi-fermion interaction takes the form,

$$U = \psi_{1,L}^{m_1} \psi_{1,R}^{n_1} \psi_{2,L}^{m_2} \psi_{2,R}^{n_2}. \quad (71)$$

where $m_{1,2}, n_{1,2} \in \mathbb{Z}$. If m_i and n_i take negative value, this represents $(\psi_{i,L}^\dagger)^{|m_i|}$ and $(\psi_{i,R}^\dagger)^{|n_i|}$ in U . Define $L_1 = m_1 + n_1$ and $L_2 = m_2 + n_2$, then $L_1 = -L_2 = M$ is required by charge conservation symmetry. Under Z_N symmetry, we find that

$$Z_N U Z_N^{-1} = e^{i\frac{2\pi}{N}[J(L_1+L_2)+kL_2]} U = e^{-i\frac{2\pi}{N}kM} U \quad (72)$$

Therefore, to make U invariant under Z_N , we require

$$kM \equiv 0 \pmod{N} \quad \Rightarrow \quad M = \frac{LCM(N, k)}{k}. \quad (73)$$

where $LCM(N, k)$ is the least common multiple of N and k . Physically, M is the number of electrons that tunnel from channel 1 to channel 2. When U is large and relevant under RG, the electron number in each channel is well-defined modulo M , which signals an emergent Z_M fermion parity symmetry. In the following, we will discuss two special situations of Eq. 73:

- **When $LCM(N, k) = N$, $M = \frac{N}{k} \in \mathbb{Z}$. Then Z_N symmetry leads to an emergent $Z_{\frac{N}{k}}$ fermion parity.** For the DSM nanowire model in the main text, we have $N = 4$ and $k = \frac{3}{2} - (-\frac{1}{2}) = 2$. Thus, $M = LCM(4, 2)/2 = 2$, which corresponds to an emergent Z_2 fermion parity.
- **When $LCM(N, k) = Nk$, $M = N$. Then Z_N symmetry leads to an emergent Z_N fermion parity.** As an example, we consider a system where $\psi_{1,L/R}$ carries angular momentum $\frac{1}{2}$, while $\psi_{2,L/R}$ carries angular momentum $-\frac{1}{2}$. For $N = 4$, now we have $k = \frac{1}{2} - (-\frac{1}{2}) = 1$ and $M = LCM(4, 1)/1 = 4$. This leads to an emergent Z_4 fermion parity.

APPENDIX I. EMERGENT Z_2 FERMION PARITY FROM 2D POINT GROUPS

Given a Z_N group and its representations, we have shown in the previous section that an Z_M fermion parity symmetry will emerge for each representation even when the total number of electrons is conserved, which is summarized in Eq. 73. In this section, we hope to look at the problem from a different perspective: Given a group G , we are wondering what representations of G could lead to an emergent Z_2 fermion parity symmetry ($M = 2$). In particular, we hope to go beyond Z_N symmetry and explore a general symmetry group G . We first propose three criteria that G should satisfy:

- G is “on-site”.** In a quasi-1D nanowire system growing along x direction, only symmetry operations that act trivially on x can be viewed as on-site symmetries. This implies that our target symmetry groups should be 2D point groups.
- Z_2 is a subgroup of G .** When this condition is satisfied, there exist two inequivalent 1D irreps with basis functions $|J\rangle$ and $|J+k\rangle$ such that $M = LCM(N, k)/k = 2$.
- There exists an interaction g such that: (i) g describes pair-hopping process between $Z_2 = \pm 1$ representations; (ii) g respects every symmetry operation in G .**

There are in total 10 point groups in 2D lattice systems: C_n and D_n , where $n = 1, 2, 3, 4, 6$. Here C_n group contains a n -fold rotation symmetry as the group generator. D_n group contains an additional in-plane mirror operation compared to C_n group. Notice that $C_1 = \{e\}$ is a trivial identity group, while $D_1 = \{e, M\}$ where M is a mirror operation.

I.1. C_n group

A C_n group is just a Z_n group. C_n groups have only 1D irreps labeled by angular momentum J , where J is integer (half-integer) for spinless (spinful) electrons. Starting from Eq. 73, we have $M = 2$ for Z_2 fermion parity. Thus, $LCM(n, k) = 2k$ and we have $n = 2k$, which leads to

$$e^{i\frac{2\pi}{n}(J'-J)} = e^{i\frac{2\pi}{n}k} = -1 \quad (74)$$

In the following, we give a detailed discussion of all C_n groups and check their compatibility with Eq. 74. These results are summarized in Table I.

- **C_2 group (spinless)** - There are two inequivalent 1D irreps: $|J=0\rangle$ and $|J=1\rangle$, which satisfies Eq. 74
- **C_2 group (spinful)** - The 1D irreps are $|J=\frac{1}{2}\rangle$ and $|J=-\frac{1}{2}\rangle$ and satisfies Eq. 74.
- **C_3 group (spinless)** - The 1D irreps are $|J=-1\rangle$, $|J=0\rangle$ and $J=1\rangle$. None of them satisfy Eq. 74.
- **C_3 group (spinful)** - The 1D irreps are $|J=-\frac{1}{2}\rangle$, $|J=\frac{1}{2}\rangle$ and $J=\frac{3}{2}\rangle$. None of them satisfy Eq. 74.

	C_2	C_3	C_4	C_6
Spinless:	$ J = 0, 1\rangle$	N/A	$ J = 0, 2\rangle$ $ J = \pm 1\rangle$	$ J = 0, 3\rangle$ $ J = 1, -2\rangle$ $ J = 2, -1\rangle$
Spinful:	$ J = \pm \frac{1}{2}\rangle$	N/A	$ J = \frac{1}{2}, -\frac{3}{2}\rangle$ $ J = -\frac{1}{2}, \frac{3}{2}\rangle$	$ J = \frac{1}{2}, -\frac{5}{2}\rangle$ $ J = \pm \frac{3}{2}\rangle$ $ J = \frac{5}{2}, -\frac{1}{2}\rangle$

TABLE I. C_n group

- **C_4 group (spinless)** - The 1D irreps are $|J = 0\rangle$, $|J = \pm 1\rangle$, and $|J = 2\rangle$. It is easy to check that both $\{|J = 0\rangle, |J = 2\rangle\}$ and $\{|J = 1\rangle, |J = -1\rangle\}$ satisfy Eq. 74.
- **C_4 group (spinful)** - The 1D irreps are $|J = \pm \frac{1}{2}\rangle$ and $|J = \pm \frac{3}{2}\rangle$. It is easy to check that both $\{|J = \frac{1}{2}\rangle, |J = -\frac{3}{2}\rangle\}$ and $\{|J = -\frac{1}{2}\rangle, |J = \frac{3}{2}\rangle\}$ satisfy Eq. 74.
- **C_6 group (spinless)** - The 1D irreps are $|J = 0\rangle$, $|J = \pm 1\rangle$, $|J = \pm 2\rangle$, and $|J = 3\rangle$. It is easy to check that $\{|J = 0\rangle, |J = 3\rangle\}$, $\{|J = -1\rangle, |J = 2\rangle\}$ and $\{|J = -2\rangle, |J = 1\rangle\}$ satisfy Eq. 74.
- **C_6 group (spinful)** - The 1D irreps are $|J = \pm \frac{1}{2}\rangle$, $|J = \pm \frac{3}{2}\rangle$, and $|J = \pm \frac{5}{2}\rangle$. It is easy to check that $\{|J = \frac{1}{2}\rangle, |J = -\frac{5}{2}\rangle\}$, $\{|J = \frac{3}{2}\rangle, |J = -\frac{3}{2}\rangle\}$ and $\{|J = \frac{5}{2}\rangle, |J = -\frac{1}{2}\rangle\}$ satisfy Eq. 74.

12. D_n group

With an additional mirror operation, irreps of D_n group can be characterized by either angular momentum J or mirror eigenvalue m , while we will continue to use J to label representations. For $n > 2$, D_n group is non-Abelian due to the non-commutation between rotation symmetry C_n and mirror symmetry M , giving rise to 2D irreps. In the following, we first derive a general condition (Eq. 80) for D_n group and pair-hopping interactions, and then apply this condition to each D_n group. Given a state $|J\rangle$, we have

$$M|J\rangle = c|-J\rangle \quad (75)$$

Here $c = 1$ for spinless electrons and $c = i$ for spinful electrons. In the basis $\Psi_{L/R} = (\psi_{J,L/R}, \psi_{-J,L/R})^T$, the symmetry operations are

$$C_n = e^{i\frac{2\pi}{n}J\sigma_z}, \quad M = \sigma_x \quad (76)$$

The pair-hopping interaction between different irreps is

$$V_{pair} = \psi_{J,L}^\dagger \psi_{J,R}^\dagger \psi_{-J,L} \psi_{-J,R} + h.c. = \Psi_L^\dagger \sigma_+ \Psi_L \Psi_R^\dagger \sigma_+ \Psi_R + h.c. \quad (77)$$

where $\sigma_\pm = \sigma_x \pm i\sigma_y$ are the pseudo-spin Pauli matrices. It is important to check the compatibility between V_{pair} and symmetry operations. Notice that

$$\begin{aligned} M\sigma_+M^{-1} &= \sigma_- \\ C_n\sigma_+C_n^{-1} &= e^{i\frac{4\pi}{n}J}\sigma_+ \end{aligned} \quad (78)$$

Therefore,

$$\begin{aligned} MV_{pair}M^{-1} &= V_{pair} \\ C_nV_{pair}C_n^{-1} &= e^{i\frac{8\pi}{n}J}V_{pair} \end{aligned} \quad (79)$$

Under n -fold rotation symmetry, V_{pair} is invariant when the following conditions are satisfied,

$$\begin{aligned} 4J &= kn, \quad k \in \mathbb{Z} \\ 2J &< n \end{aligned} \quad (80)$$

	D_1	D_2	D_3	D_4	D_6
Spinless: $ M = \pm 1\rangle$	$ J = 0, 1\rangle$	N/A	$ J = \pm 1\rangle$	N/A	
Spinful: $ M = \pm i\rangle$	$ J = \pm \frac{1}{2}\rangle$	N/A	N/A	$ J = \pm \frac{3}{2}\rangle$	

TABLE II. D_n group

The second condition in Eq. 80 guarantees that $|J\rangle$ and $|-J\rangle$ are different states.

Meanwhile, we can reformulate our argument from mirror symmetry eigenstates

$$|m_{\pm}\rangle = \frac{1}{\sqrt{2}}(|J\rangle \pm |-J\rangle) \quad (81)$$

where $M|m_{\pm} = \pm|m_{\pm}\rangle$. In this case, we could define the pair-hopping interaction under a new basis $\tilde{\Psi}_{L/R} = (\psi_{m_+,L/R}, \psi_{m_-,L/R})^T$,

$$\tilde{V}_{pair} = \tilde{\Psi}_L^\dagger \sigma_+ \tilde{\Psi}_L \tilde{\Psi}_R^\dagger \sigma_+ \tilde{\Psi}_R + h.c. \quad (82)$$

In this case, the symmetry operations are

$$\tilde{C}_n = e^{i\frac{2\pi}{n}J\sigma_x}, \quad \tilde{M} = c\sigma_z. \quad (83)$$

It is easy to see that V_{pair} must satisfy Eq. 80 to respect symmetries. The results of our detailed analysis below is summarized in Table II.

- **D_1 group (spinless)** - D_1 group has no rotational symmetry operation, so we use mirror eigenvalue to label 1D irreps of D_1 group as $|m = 1\rangle$ and $|m = -1\rangle$, which satisfies our requirement for hosting Majorana.
- **D_1 group (spinful)** - The D_1 double group is similar to its spinless version. The 1D irreps that will work are $|m = i\rangle$ and $|m = -i\rangle$.
- **D_2 group (spinless)** - This is similar to the case of spinless C_2 group, and the 1D irreps are $|J = 0\rangle$ and $|J = 1\rangle$.
- **D_2 group (spinful)** - Different from the spinless D_2 group, $|J = \frac{1}{2}\rangle$ and $|J = -\frac{1}{2}\rangle$ form a 2D irrep since $M|J = \frac{1}{2}\rangle = i|J = -\frac{1}{2}\rangle$. It is easy to see that $|J = \frac{1}{2}\rangle$ and $|J = -\frac{1}{2}\rangle$ satisfy Eq. 80.
- **D_3 group (spinless & spinful)** - For $n = 3$, Eq. 80 becomes: $4J = 3k$ and $J < \frac{3}{2}$. It is easy to check that for both spinless (J is integer) and spinful (J is half-integer) cases, there is no J satisfying both equations.
- **D_4 group (spinless & spinful)** - For $n = 4$, it is easy to check that Eq. 80 becomes: $J = k$ and $J < 2$. Thus, J can only take integer values $J = 1$, which corresponds to the spinless case.
- **D_6 group (spinless & spinful)** - For $n = 6$, Eq. 80 is: $2J = 3k$ and $J < 3$. The only solution is $J = \frac{3}{2}$.

APPENDIX J. DIAGONALIZING H_- WITH MODE EXPANSION

In this appendix, we introduce mode expansion technique to explicitly diagonalize the anti-bonding Hamiltonian H_- . The mode expansion offers us a powerful weapon to attack the electron tunneling problem. We introduce,

$$\begin{aligned} \phi_-(x) &= \sqrt{\frac{\pi}{2}}(n_\phi + \frac{1}{2}) + \sqrt{\frac{\pi}{2}}\frac{\Delta n x}{L} + \frac{1}{\sqrt{\pi}} \sum_{k=1}^{\infty} \sqrt{\frac{1}{K-k}} \sin \frac{\pi k x}{L} (a_k + a_k^\dagger) \\ \theta_-(x) &= \sqrt{\frac{\pi}{2}}(n_\theta + \frac{1}{2}) + \sqrt{\frac{\pi}{2}}\theta_0 - i\frac{1}{\sqrt{\pi}} \sum_{k=1}^{\infty} \sqrt{\frac{K-k}{k}} \cos \frac{\pi k x}{L} (a_k - a_k^\dagger) \end{aligned} \quad (84)$$

with $[\Delta n, \theta_0] = i$ and $[a_k, a_{k'}^\dagger] = \delta_{k,k'}$. Here, we have expanded the cosine term in H_- around its minimum as $4\pi g[\theta_- - (n_\theta + \frac{1}{2})\sqrt{\frac{\pi}{2}}]^2$. Plug in the mode expansion (Eq. 84) to the Hamiltonian and after some tedious calculations, we obtain that

$$\begin{aligned} \frac{v}{2}K_- \int dx (\partial_x \phi_-)^2 &= \frac{v\pi}{4L}(\Delta n)^2 + \sum_k \frac{v\pi k}{4L} [a_k a_k^\dagger + a_k^\dagger a_k + (a_k)^2 + (a_k^\dagger)^2] \\ \frac{v}{2}K_- \int dx (\partial_x \theta_-)^2 &= - \sum_k \frac{v\pi k}{4L} [-a_k a_k^\dagger - a_k^\dagger a_k + (a_k)^2 + (a_k^\dagger)^2] \\ 4\pi g[\theta_- - (n_\theta + \frac{1}{2})\sqrt{\frac{\pi}{2}}]^2 &= 2gL\pi^2\theta_0^2 - \sum_k \frac{2gLK_-}{k} [-a_k a_k^\dagger - a_k^\dagger a_k + (a_k)^2 + (a_k^\dagger)^2] \end{aligned} \quad (85)$$

Therefore,

$$H_- = \frac{v\pi}{4L}(\Delta n)^2 + 2gL\pi^2\theta_0^2 + \sum_k \frac{A_k}{2} [a_k a_k^\dagger + a_k^\dagger a_k] - \sum_k \frac{B_k}{2} [(a_k)^2 + (a_k^\dagger)^2]. \quad (86)$$

With

$$\begin{aligned} A_k &= \frac{v\pi k}{L} + \frac{4gLK_-}{k} \\ B_k &= \frac{4gLK_-}{k} \end{aligned} \quad (87)$$

Introduce the following Bogoliubov transformations

$$\begin{aligned} \Delta n &= \left(\frac{8g\pi L^2}{v}\right)^{\frac{1}{4}} \frac{d + d^\dagger}{\sqrt{2}} \\ \theta_0 &= \left(\frac{8g\pi L^2}{v}\right)^{-\frac{1}{4}} \frac{d - d^\dagger}{i\sqrt{2}} \\ a_k &= C_k \alpha_k + D_k \alpha_k^\dagger \end{aligned} \quad (88)$$

where $C_k = \sqrt{\frac{1}{2}(\frac{A_k}{E_k} + 1)}$ and $D_k = \sqrt{\frac{1}{2}(\frac{A_k}{E_k} - 1)}$. The Bogoliubov quasi-particles satisfy commutation relations as $[d, d^\dagger] = 1$ and $[\alpha_k, \alpha_{k'}^\dagger] = \delta_{k,k'}$. The energy function E_k is now given by $E_k = \sqrt{A_k^2 - B_k^2}$, and it is closely related to the energy dispersion of the system

$$H_- = \sqrt{\frac{vg\pi^3}{2}} d^\dagger d + \sum_k E_k \alpha_k^\dagger \alpha_k \quad (89)$$

Let us have a closer look at the form of E_k . By defining $q = \frac{\pi k}{L}$, we find a very nice form

$$E_k = \sqrt{v^2 q^2 + \Delta^2} \quad (90)$$

where $\Delta = \sqrt{8\pi vgK_-}$ physically denotes the energy gap formed in the anti-bonding sector, which originates from pair-hopping interaction g .

APPENDIX K. TRANSITION AMPLITUDE OF ELECTRON TUNNELING PROBLEM

When an electron of $s = 1$ tunnels into the system, it changes the sign of both total fermion parity P_{tot} and $P^{(2)}$. Therefore, the original ground state $|0\rangle = |N, p\rangle$ is changed to $|1\rangle = |N + 1, -p\rangle$ via this tunneling process, with $p \in \pm 1$. On the other hand, the total charge Q_+ and the charge in channel $s = 1$ are given by

$$\begin{aligned} Q_+ &= \sqrt{\frac{2}{\pi}} [\phi_+(L) - \phi_+(0)], \\ Q_1 &= \sqrt{\frac{1}{\pi}} [\phi_1(L) - \phi_1(0)] = \frac{1}{2}(Q_+ + Q_-) \end{aligned} \quad (91)$$

Since $\Delta Q_+ = \Delta Q_1 = 1$ during this single electron tunneling, we find that $\Delta Q_+ = \Delta Q_- = 1$, or equivalently

$$\delta\phi_+ = \delta\phi_- = \sqrt{\frac{\pi}{2}}. \quad (92)$$

where we have defined $\delta\phi_{\pm} = \phi_{\pm}(L) - \phi_{\pm}(0)$. Here it is convenient to parameterize $\Delta\phi_{\pm}(x) = \sqrt{\frac{\pi}{2}}(1 - \frac{x}{L})$. The two ground states can be connected via a unitary transformation $|1\rangle = e^{-i\eta}|0\rangle$ [36], where $\eta = \eta_+ + \eta_-$ and

$$\begin{aligned} \eta_+ &= \int dx \Delta\phi_+ \partial_x \theta_+ \\ \eta_- &= \int dx \Delta\phi_- \partial_x \theta_- \end{aligned} \quad (93)$$

With the fact that $[e^{-i\eta_{\pm}}, \phi_{\pm}(x)] = \Delta\phi_{\pm}(x)e^{-i\eta_{\pm}}$, it is easy to show that $e^{-i\eta_{\pm}}\phi_{\pm}(x)e^{i\eta_{\pm}} = \phi_{\pm}(x) + \Delta\phi_{\pm}(x)$.

Next, we would like to calculate the tunneling amplitude

$$\begin{aligned} \langle 1|\psi_{1,R}^{\dagger}|0\rangle &= \langle 0|e^{i\eta}e^{-i\sqrt{\pi}(\phi_1-\theta_1)}|0\rangle \\ &= \langle e^{i\eta_+}e^{-i\sqrt{\frac{\pi}{2}}(\phi_+-\theta_+)}\rangle_+ \times \langle e^{i\eta_-}e^{-i\sqrt{\frac{\pi}{2}}(\phi_--\theta_-)}\rangle_- \\ &= T_+T_- \end{aligned} \quad (94)$$

Let us first focus on the anti-bonding part,

$$\begin{aligned} T_- &= \langle e^{i\eta_-}e^{-i\sqrt{\frac{\pi}{2}}(\phi_--\theta_-)}\rangle_- \\ &= e^{-\frac{1}{2}\langle[\eta_- - \sqrt{\frac{\pi}{2}}(\phi_--\theta_-)]^2\rangle_-} \end{aligned} \quad (95)$$

K1. Contribution from T_-

With the mode expansion in Eq. 84, let us move on to calculate T_- . For δ_-

$$\begin{aligned} \eta_- &= \int dx \Delta\phi_- \partial_x \theta_- \\ &= \frac{i}{\sqrt{2}} \sum_k \sqrt{\frac{K}{k}} \frac{\pi k}{L} (a_k - a_k^{\dagger}) \int_0^L dx (1 - \frac{x}{L}) \sin \frac{\pi k x}{L} \\ &= i \sqrt{\frac{K}{2}} \sum_k \frac{a_k - a_k^{\dagger}}{\sqrt{k}} \end{aligned} \quad (96)$$

Notice that in $T_- = e^{-F_-}$, the imaginary part in $F_- = \frac{1}{2}\langle[\eta_- - \sqrt{\frac{\pi}{2}}(\phi_--\theta_-)]^2\rangle_-$ only contributes to a phase factor, while its amplitude originates from its real part. By ignoring the imaginary part, we find that

$$F_- = \frac{1}{2}\langle[\eta_- + \sqrt{\frac{\pi}{2}}\theta_-]^2\rangle_- + \frac{\pi}{4}\langle\phi_-^2\rangle_- \quad (97)$$

To start with

$$\eta_- + \sqrt{\frac{\pi}{2}}\theta_- = i \sum_k \sqrt{\frac{K_-}{2k}} (a_k - a_k^{\dagger}) (1 - \cos \frac{\pi k x}{L}) + \frac{\pi}{2}(n_{\theta} + \theta_0 + \frac{1}{2}) \quad (98)$$

In the following discussion, we will ignore the θ_0 and Δn part, which will give rise to a universal contribution to T_- as

$$e^{-\frac{\pi^2}{8}[(n_{\theta}+\frac{1}{2})^2+(n_{\phi}+\frac{1}{2})^2]} \times e^{-\frac{\pi^2}{16L}(\sqrt{\frac{v}{8g\pi}}+\sqrt{\frac{8g\pi}{v}}x^2)} \quad (99)$$

where the second term becomes unity as $L \rightarrow \infty$. Then

$$\begin{aligned} \langle[\eta_- + \sqrt{\frac{\pi}{2}}\theta_-]^2\rangle_- &= - \sum_{k,k'} \frac{K_-}{2} \frac{1}{\sqrt{k k'}} (1 - \cos \frac{\pi k x}{L}) (1 - \cos \frac{\pi k' x}{L}) (a_k - a_k^{\dagger})(a_{k'} - a_{k'}^{\dagger}) \\ &= \sum_k (C_k - D_k)^2 \frac{K_-}{2k} (1 - \cos \frac{\pi k x}{L})^2 \end{aligned} \quad (100)$$

where we have used $\langle \alpha_k^\dagger \alpha_k \rangle = 0$. Let us define $\kappa = \xi^{-1} = \frac{\Delta}{v}$, and the correlation length is defined as

$$\xi = \frac{v}{\Delta} = \sqrt{\frac{v}{8\pi g K_-}}. \quad (101)$$

Then we have

$$\begin{aligned} A_k &= vq + \frac{\Delta^2}{2qv} = v\left(q + \frac{\kappa^2}{2q}\right) \\ B_k &= v\frac{\kappa^2}{2q} \end{aligned} \quad (102)$$

In the strong coupling limit $\Delta \rightarrow \infty$, $\kappa \gg q$. Then $A_k \approx B_k \approx v\frac{\kappa^2}{2q}$ and $E_k \approx v\kappa$. We find that

$$(C_k - D_k)^2 \approx \frac{q}{\kappa} \quad (103)$$

By taking $L \rightarrow \infty$,

$$\begin{aligned} \frac{1}{2} \langle [\eta_- + \sqrt{\frac{\pi}{2}} \theta_-]^2 \rangle_- &= \frac{K_-}{4\kappa} \int dq (1 - \cos qx)^2 \times e^{-\epsilon q} \\ &= \frac{3K_- \xi}{8 \epsilon} \end{aligned} \quad (104)$$

where we have introduced a decay factor $e^{-\epsilon q}$ as the short distance divergence, and ϵ is the short distance cut-off. Therefore, this part of F_- does not have spatial dependence. For the second part of F_- ,

$$\begin{aligned} \frac{\pi}{4} \langle \phi_-^2 \rangle_- &= \frac{1}{4K_-} \sum_{k,k'} \sqrt{\frac{1}{kk'}} \sin \frac{\pi kx}{L} \sin \frac{\pi k'x}{L} (a_k + a_k^\dagger)(a_{k'} + a_{k'}^\dagger) \times e^{-\epsilon q} \\ &= \frac{1}{4K_-} \sum_k \frac{(C_k + D_k)^2}{k} \sin^2 \frac{\pi kx}{L} \times e^{-\epsilon q} \\ &= \frac{\kappa}{4K_-} \int dq \frac{\sin^2 qx}{q^2} \times e^{-\epsilon q} \\ &= \frac{\kappa}{4K_-} \left[x \arctan \frac{2x}{\epsilon} - \frac{1}{4} \epsilon \log \left(\frac{4x^2 + \epsilon^2}{\epsilon^2} \right) \right] \\ &= \frac{\pi}{8K_- \xi} x - \frac{\epsilon}{8K_- \xi} \log \frac{2x}{\epsilon} \end{aligned} \quad (105)$$

Finally, we arrive at the following important result,

$$T_- \sim \left(\frac{2x}{\epsilon} \right)^{\frac{\epsilon}{8K_- \xi}} \times e^{-\frac{\pi}{8K_- \xi} x} \quad (106)$$

K2. Contribution from T_+

Since the bonding part is gapless, we expect it only gives a power-law correction to T . To see this, we notice that the essential difference between bonding and anti-bonding physics lies in the existence of g . By setting $g = 0$ in anti-bonding sector, one should be able to recover the physics in the bonding sector. In this limit, we find that

$$\Delta = 0, \quad E_k = A_k = vq, \quad B_k = 0. \quad (107)$$

This gives rise to $C_k = 1$ and $D_k = 0$. Then

$$\begin{aligned} \frac{1}{2} \langle [\eta_+ + \sqrt{\frac{\pi}{2}} \theta_+]^2 \rangle_+ &= \frac{K_+}{4} \int dq \frac{(1 - \cos qx)^2}{q} \times e^{-\epsilon q} \\ &= \frac{K_+}{4} \left[\log \frac{x^2 + \epsilon^2}{\epsilon^2} - \frac{1}{4} \log \frac{4x^2 + \epsilon^2}{\epsilon^2} \right] \end{aligned} \quad (108)$$

and

$$\begin{aligned} \frac{\pi}{4} \langle \phi_+^2 \rangle_+ &= \frac{1}{4K_+} \int dq \frac{\sin^2 qx}{q} \times e^{-\epsilon q} \\ &= \frac{1}{16K_+} \log \frac{4x^2 + \epsilon^2}{\epsilon^2} \end{aligned} \quad (109)$$

Then we arrive at

$$T_+ = \left(\frac{\epsilon^2}{x^2 + \epsilon^2} \right)^{\frac{K_+}{4}} \left(\frac{4x^2 + \epsilon^2}{\epsilon^2} \right)^{\frac{1}{16} (K_+ - \frac{1}{K_+})} \quad (110)$$

Together with the anti-bonding contribution, we conclude that the single electron tunneling amplitude is given by

$$\langle 1 | \psi_{1,R}^\dagger | 0 \rangle = \mathcal{N}(x, \epsilon, K_\pm) e^{-\frac{\pi}{8K_-} \frac{x}{\epsilon}}. \quad (111)$$

where $\mathcal{N}(x, \epsilon, K_\pm)$ denotes the power-law corrections.

APPENDIX L. GENERAL FORMALISM OF DEBC METHOD

In this appendix, we briefly review the general formalism of “delayed evaluation of boundary condition” (DEBC) method [39], and how this method can help us to evaluate scaling dimension of operators with given boundary conditions. To start with, let us consider N quantum wires with different Luttinger parameter K_i ($i = 1, 2, \dots, N$) meet at $x = 0$ and form a junction. The bosonized Hamiltonian is given by

$$H = \sum_{i=1}^N \int dx [K_i (\partial_x \phi_i)^2 + \frac{1}{K_i} (\partial_x \theta_i)^2] \quad (112)$$

where abelian bosonization is defined as

$$\begin{aligned} \psi_{i,R} &\sim e^{i\sqrt{\pi}\chi_{i,R}} = e^{i\sqrt{\pi}(\phi_i - \theta_i)} \\ \psi_{i,L} &\sim e^{-i\sqrt{\pi}\chi_{i,L}} = e^{-i\sqrt{\pi}(\phi_i + \theta_i)} \end{aligned} \quad (113)$$

It is convenient to rescale the dual fields to make the system effectively non-interacting,

$$\begin{aligned} \tilde{\phi}_i &= \sqrt{K_i} \phi_i, \quad \tilde{\theta}_i = \frac{1}{\sqrt{K_i}} \theta_i \\ \tilde{\chi}_{i,R} &= \tilde{\phi}_i - \tilde{\theta}_i, \quad \tilde{\chi}_{i,L} = \tilde{\phi}_i + \tilde{\theta}_i \end{aligned} \quad (114)$$

The boundary condition is demonstrated by

$$\vec{\chi}_R = \mathcal{O} \vec{\chi}_L \quad (115)$$

where $\vec{\chi}_{R/L} = (\tilde{\chi}_{1,R/L}, \tilde{\chi}_{2,R/L}, \dots, \tilde{\chi}_{N,R/L})^T$. \mathcal{O} is an orthogonal matrix with $\mathcal{O}\mathcal{O}^T = 1$, which contains key information of boundary condition. In other words, **a particular choice of \mathcal{O} determines certain type of conformal invariant boundary condition, which corresponds to certain RG fixed point in the tunneling phase diagram.**

To be specific, perturbations of a boundary fixed point come from tunneling or backscattering process, which generally can be written as

$$g_{m,n} \sim e^{i\sqrt{\pi}(\mathbf{m} \cdot \vec{\phi} + \mathbf{n} \cdot \vec{\theta})} \quad (116)$$

where $\vec{\phi} = (\tilde{\phi}_1, \tilde{\phi}_2, \dots, \tilde{\phi}_N)^T$ and $\vec{\theta} = (\tilde{\theta}_1, \tilde{\theta}_2, \dots, \tilde{\theta}_N)^T$. With the definition of \mathcal{O} matrix, the boundary condition can be easily implemented in the $\tilde{\chi}_{R,L}$ basis. Thus,

$$\begin{aligned} g_{m,n} &\sim e^{i\frac{\sqrt{\pi}}{2}[(\mathbf{m}+\mathbf{n}) \cdot \vec{\chi}_R + (\mathbf{m}-\mathbf{n}) \cdot \vec{\chi}_L]} \\ &= e^{i\frac{\sqrt{\pi}}{2}[\mathcal{O}^T(\mathbf{m}+\mathbf{n}) + (\mathbf{m}-\mathbf{n})]^T \vec{\chi}_L} \end{aligned} \quad (117)$$

Its scaling dimension is

$$\Delta[g_{m,n}] = \frac{1}{8} |\mathcal{O}^T(\mathbf{m} + \mathbf{n}) + (\mathbf{m} - \mathbf{n})|^2 \quad (118)$$

The specific form of \mathcal{O} depends on the boundary condition we impose.

L1. Orthogonality of \mathcal{O} matrix

The orthogonality condition turns out to be an important and strong constraint to \mathcal{O} , which can be proved as follows. Consider an operator $g_{A,B} = e^{i\frac{\sqrt{\pi}}{2}(\mathbf{A}\cdot\vec{\chi}_R + \mathbf{B}\cdot\vec{\chi}_L)}$, with \mathbf{A} and \mathbf{B} both N -component vectors. From Eq. 115, $\vec{\chi}_L = \mathcal{O}^{-1}\vec{\chi}_R$. Then

$$\begin{aligned} g_{A,B} &= e^{i\frac{\sqrt{\pi}}{2}(\mathbf{A}^T\mathcal{O} + \mathbf{B}^T)\vec{\chi}_L} \\ &= e^{i\frac{\sqrt{\pi}}{2}(\mathbf{A}^T + \mathbf{B}^T\mathcal{O}^{-1})\vec{\chi}_R} \end{aligned} \quad (119)$$

In terms of $\vec{\chi}_L$, the scaling dimension of $g_{A,B}$ is

$$\begin{aligned} \Delta(g_{A,B}) &= \frac{1}{8}|\mathbf{A}^T\mathcal{O} + \mathbf{B}^T|^2 \\ &= \frac{1}{8}[\mathcal{O}^T(\mathbf{A}\mathbf{A}^T)\mathcal{O} + \mathbf{B}\mathbf{B}^T + \mathcal{O}^T\mathbf{A}\mathbf{B}^T + \mathbf{B}\mathbf{A}^T\mathcal{O}] \\ &= \frac{1}{8}[|\mathbf{A}|^2\mathcal{O}^T\mathcal{O} + |\mathbf{B}|^2 + (\mathcal{O}^T + \mathcal{O})\mathbf{A}\cdot\mathbf{B}] \end{aligned} \quad (120)$$

In terms of $\vec{\chi}_R$, we find that

$$\begin{aligned} \Delta(g_{A,B}) &= \frac{1}{8}|\mathbf{A}^T + \mathbf{B}^T\mathcal{O}^{-1}|^2 \\ &= \frac{1}{8}[|\mathbf{A}|^2 + (\mathcal{O}\mathcal{O}^T)^{-1}|\mathbf{B}|^2 + (\mathcal{O} + \mathcal{O}^T)^{-1}\mathbf{A}\cdot\mathbf{B}]. \end{aligned} \quad (121)$$

To make Eq. 120 and Eq. 121 self-consistent, orthogonality condition $\mathcal{O}\mathcal{O}^T = 1$ must be satisfied.

L2. Application of DEBC to 2LL/LL junction

Now, we are ready to apply the DEBC method to our 2LL/LL junction setup. The central task here is to identify \mathcal{O} matrix that characterizes physical RG fixed point. Across the junction, current conservation requires

$$J_{x<0} + J_{x>0} = 0 \quad (122)$$

Here $J_{x<0} = -\sqrt{\frac{1}{\pi}}\partial_t\phi_0$ and $J_{x>0} = -\sqrt{\frac{1}{\pi}}\partial_t(\phi_1 + \phi_2) = \sqrt{\frac{2}{\pi}}\partial_t\phi_+$. The rescaling rule of fields can be defined similar to Eq. 114, with $i = 0, \pm$. Then the current conservation condition becomes

$$\partial_t\left(\frac{1}{\sqrt{K_0}}\tilde{\phi}_0 + \sqrt{\frac{2}{K_+}}\tilde{\phi}_+\right) = 0 \quad (123)$$

Other information of \mathcal{O} depends on the details of boundary conditions. Once we obtain \mathcal{O} , it is important to write down possible tunneling or backscattering operators that could perturb the fixed point.

(i) *Single electron tunneling,*

$$T_{ij}^s = \psi_{i,R}^\dagger\psi_{j,L} + h.c. \sim \cos\sqrt{\pi}[(\phi_i + \phi_j) - (\theta_i - \theta_j)], \quad (124)$$

where $i \neq j \in \{0, 1, 2\}$. However, electron tunneling process should conserve angular momentum. Let us consider a case where electron from LL lead can hop to both $i = 1$ and $i = 2$. But inter-channel single electron tunneling events (T_{12}^s and T_{21}^s) in 2LL are strictly forbidden due to the angular momentum conservation.

(ii) *Single electron backscattering,*

$$B_i = \psi_{i,L}^\dagger\psi_{i,R} + h.c. \sim \cos 2\sqrt{\pi}\phi_i, \quad (125)$$

with $i \in \{0, 1, 2\}$.

(iii) *Pair electron tunneling,*

$$T_{ij}^p = \psi_{i,R}^\dagger\psi_{i,L}^\dagger\psi_{j,R}\psi_{j,L} + h.c. \sim \cos 2\sqrt{\pi}(\theta_i - \theta_j) \quad (126)$$

with $i < j \in \{0, 1, 2\}$. Notice that the pair electron tunneling is essentially different from T_{ij}^2 .

APPENDIX M. PHASE DIAGRAM OF MAJORANA-FREE 2LL/LL JUNCTION

In this section, let us first ignore pair hopping interaction between $i = 1$ and $i = 2$ that pins θ_- . Then the system is very similar to a conventional ‘‘Y’’ junction composed of three independent quantum wires, while rMZM does NOT show up at the junction. However, an important difference from previous work [39, 40] comes from the constraint of angular momentum conservation. In particular, electron tunneling between $i = 1$ and $i = 2$ is forbidden to conserve angular momentum. For our purpose, we will focus on the situation where $K_- < 1$.

To identify a fixed point, an effective way is to assume that some electron operators have vanishing scaling dimensions. This ansatz immediately leads to a corresponding \mathcal{O} matrix. With this \mathcal{O} matrix, we first check its orthogonality condition to verify its validity. A stable fixed point is confirmed when all possible perturbations are found to be irrelevant, with the help of Eq. 118. Below, we first use ‘‘disconnecting fixed point’’ as a detailed example to demonstrate how DEBC method extracts the information of a fixed point. Then we will exhaust all physical RG fixed points and discuss their stability problem.

M1. Disconnecting fixed point: an tutorial of DEBC method

The disconnecting fixed point is characterized by the vanishing scaling dimension of all the backscattering processes $B_{0,1,2}$. Thanks to the current conservation, the vanishing scaling dimension of two backscattering operators will automatically leads to zero scaling dimension of the remaining backscattering operator. Physically, this simply means that if channel $i = 0$ and $i = 1$ are both disconnected, $i = 2$ is also forced to be disconnected at the junction as no electron can flow from $i = 0, 1$ to $i = 2$.

We first define $\vec{\chi}_{R/L} = (\tilde{\chi}_{0,R/L}, \tilde{\chi}_{+,R/L}, \tilde{\chi}_{-,R/L})^T$, following the convention in Eq. 114. The backscattering operators are now:

$$\begin{aligned} B_0 &\sim \cos \sqrt{\pi} \left(\frac{\tilde{\chi}_{0,R} + \tilde{\chi}_{0,L}}{\sqrt{K_0}} \right) \\ B_1 &\sim \cos \sqrt{\pi} \left[\frac{\tilde{\chi}_{+,R} + \tilde{\chi}_{+,L}}{\sqrt{2K_+}} + \frac{\tilde{\chi}_{-,R} + \tilde{\chi}_{-,L}}{\sqrt{2K_-}} \right] \\ B_2 &\sim \cos \sqrt{\pi} \left[\frac{\tilde{\chi}_{+,R} + \tilde{\chi}_{+,L}}{\sqrt{2K_+}} - \frac{\tilde{\chi}_{-,R} + \tilde{\chi}_{-,L}}{\sqrt{2K_-}} \right] \end{aligned} \quad (127)$$

Let us re-examine Eq. 117 and Eq. 118, the only way to make $\Delta[g_{m,n}] = 0$ is to impose

$$(\mathbf{m} + \mathbf{n}) \cdot \vec{\chi}_R + (\mathbf{m} - \mathbf{n}) \cdot \vec{\chi}_L = 0. \quad (128)$$

Therefore, we impose Eq. 128 to B_0 and B_1 . Together with the current conservation condition, we arrive at

$$\begin{aligned} \frac{\tilde{\chi}_{0,R} + \tilde{\chi}_{0,L}}{\sqrt{K_0}} &= 0 \\ \frac{\tilde{\chi}_{+,R} + \tilde{\chi}_{+,L}}{\sqrt{2K_+}} + \frac{\tilde{\chi}_{-,R} + \tilde{\chi}_{-,L}}{\sqrt{2K_-}} &= 0 \\ \frac{\tilde{\chi}_{0,R} + \tilde{\chi}_{0,L}}{2\sqrt{K_0}} + \frac{\tilde{\chi}_{+,R} + \tilde{\chi}_{+,L}}{\sqrt{2K_+}} &= 0 \end{aligned} \quad (129)$$

It is quite easy to see the solution of the above equations as

$$\tilde{\chi}_{w,R} = -\tilde{\chi}_{w,L}, \quad \forall w \in \{0, 1, 2\}, \quad (130)$$

which immediately leads to the rotation matrix \mathcal{O}_D that characterizes disconnecting fixed point according to its definition (Eq. 115):

$$\mathcal{O}_D = \begin{pmatrix} -1 & 0 & 0 \\ 0 & -1 & 0 \\ 0 & 0 & -1 \end{pmatrix}. \quad (131)$$

It is easy to see that \mathcal{O}_D is an orthogonal matrix. Physically, Eq. 130 implies

$$\phi_0 = \phi_+ = \phi_- = 0. \quad (132)$$

which is recognized as the disconnecting boundary condition at the junction. The scaling dimensions of electron operators can be calculated via Eq. 118,

$$\begin{aligned}
\Delta(T_{10}^s) &= \Delta(T_{01}^s) = \Delta(T_{20}^s) = \Delta(T_{02}^s) = \frac{1}{4}(2K_0 + K_+ + K_-) \\
\Delta(T_{01}^p) &= 2K_0 + K_+ + K_- \\
\Delta(T_{12}^p) &= 4K_- \\
\Delta(T_{20}^p) &= 2K_0 + K_+ + K_- \\
\Delta(B_0) &= 0 \\
\Delta(B_1) &= 0 \\
\Delta(B_2) &= 0.
\end{aligned} \tag{133}$$

When all tunneling terms are irrelevant, we require

$$\begin{aligned}
K_0 &> \frac{(4 - K_-) - K_+}{2} \\
K_- &> \frac{1}{4}
\end{aligned} \tag{134}$$

This condition explicitly characterizes the region in the tunneling phase diagram where DFP is stable.

M2. Pair-tunneling fixed point

At the pair-tunneling fixed point, two-electron pair-tunneling process T_{ij}^P is dominating, and

$$\mathcal{O}_P = \begin{pmatrix} -1 + \frac{4K_0}{2K_0+K_+} & -\frac{2\sqrt{2K_0K_+}}{2K_0+K_+} & 0 \\ -\frac{2\sqrt{2K_0K_+}}{2K_0+K_+} & 1 - \frac{4K_0}{2K_0+K_+} & 0 \\ 0 & 0 & 1 \end{pmatrix}. \tag{135}$$

The \mathcal{O}_P matrix is obtained similarly to \mathcal{O}_D matrix in Eq. 131 in the last section. The orthogonality of \mathcal{O}_D can be checked easily. From \mathcal{O}_P , it is easy to tell that

$$\phi_0 = -\sqrt{2}\phi_+, \quad \theta_+ = \sqrt{2}\theta_0, \quad \theta_- = 0. \tag{136}$$

The scaling dimensions at this fixed point are

$$\begin{aligned}
\Delta(T_{10}^s) &= \Delta(T_{01}^s) = \Delta(T_{20}^s) = \Delta(T_{02}^s) = \frac{1}{4}\left(\frac{1}{2K_0 + K_+} + \frac{1}{K_-}\right) \\
\Delta(T_{01}^p) &= 0 \\
\Delta(T_{12}^p) &= 0 \\
\Delta(T_{20}^p) &= 0 \\
\Delta(B_0) &= \frac{4}{2K_0 + K_+} \\
\Delta(B_1) &= \frac{1}{2K_0 + K_+} + \frac{1}{K_-} \\
\Delta(B_2) &= \frac{1}{2K_0 + K_+} + \frac{1}{K_-}.
\end{aligned} \tag{137}$$

Pair-tunneling fixed point is stable when

$$\begin{aligned}
\frac{1}{2K_0 + K_+} + \frac{1}{K_-} &> 4 \\
2K_0 + K_+ &< 4
\end{aligned} \tag{138}$$

Thus

$$K_0 < \frac{C_p - K_+}{2} \tag{139}$$

where $C_p = 4$ if $K_- \leq \frac{1}{4}$ and $C_p = \min\{4, (4 - \frac{1}{K_-})^{-1}\}$ if $K_- > \frac{1}{4}$.

M3. χ_+ fixed point

χ_+ fixed point is defined so that T_{10}^s and T_{02}^s are the only terms whose scaling dimension is vanishing, and thus dominate the junction physics. We find that

$$\mathcal{O}_+ = \frac{1}{1 + K_-(2K_0 + K_+)} \begin{pmatrix} -1 + K_-(2K_0 - K_+) & -2K_-\sqrt{2K_0K_+} & 2\sqrt{2K_0K_-} \\ -2K_-\sqrt{2K_0K_+} & -1 - K_-(2K_0 - K_+) & -2\sqrt{K_+K_-} \\ -2\sqrt{2K_0K_-} & 2\sqrt{K_+K_-} & -1 + K_-(2K_0 + K_+) \end{pmatrix}. \quad (140)$$

Despite its complicated form, one can still check that $\mathcal{O}_+\mathcal{O}_+^T = 1$ is satisfied. From \mathcal{O}_+ , this simply means

$$\phi_0 = -\sqrt{2}\phi_+ = \sqrt{2}\theta_-, \quad \phi_- = \theta_+ - \sqrt{2}\theta_0. \quad (141)$$

The scaling dimensions at this fixed point are

$$\begin{aligned} \Delta(T_{10}^s) &= \Delta(T_{02}^s) = 0 \\ \Delta(T_{01}^s) &= \Delta(T_{20}^s) = \frac{2K_0 + K_+ + K_-}{1 + K_-(2K_0 + K_+)} \\ \Delta(T_{01}^p) &= \frac{2K_0 + K_+ + K_-}{1 + K_-(2K_0 + K_+)} \\ \Delta(T_{12}^p) &= \frac{4K_-}{1 + K_-(2K_0 + K_+)} \\ \Delta(T_{20}^p) &= \frac{2K_0 + K_+ + K_-}{1 + K_-(2K_0 + K_+)} \\ \Delta(B_0) &= \frac{4K_-}{1 + K_-(2K_0 + K_+)} \\ \Delta(B_1) &= \frac{2K_0 + K_+ + K_-}{1 + K_-(2K_0 + K_+)} \\ \Delta(B_2) &= \frac{2K_0 + K_+ + K_-}{1 + K_-(2K_0 + K_+)}. \end{aligned} \quad (142)$$

χ_+ fixed point is stable when

$$\begin{aligned} [1 - (2K_0 + K_+)](1 - K_-) &< 0 \\ K_-[4 - (2K_0 + K_+)] &> 1 \end{aligned} \quad (143)$$

Since $K_- < 1$, we find that

$$\begin{aligned} \frac{1 - K_+}{2} < K_0 < \frac{(4 - \frac{1}{K_-}) - K_+}{2} \\ \text{and } K_- > \frac{1}{3} \end{aligned} \quad (144)$$

M4. χ_- fixed point

When T_{01}^s and T_{20}^s are dominating, we arrive at the χ_- fixed point, with

$$\mathcal{O}_- = \frac{1}{1 + K_-(2K_0 + K_+)} \begin{pmatrix} -1 + K_-(2K_0 - K_+) & -2K_-\sqrt{2K_0K_+} & -2\sqrt{2K_0K_-} \\ -2K_-\sqrt{2K_0K_+} & -1 - K_-(2K_0 - K_+) & 2\sqrt{K_+K_-} \\ 2\sqrt{2K_0K_-} & -2\sqrt{K_+K_-} & -1 + K_-(2K_0 + K_+) \end{pmatrix}. \quad (145)$$

and

$$\phi_0 = -\sqrt{2}\phi_+ = -\sqrt{2}\theta_-, \quad \phi_- = -\theta_+ + \sqrt{2}\theta_0. \quad (146)$$

Notice the difference and similarity between \mathcal{O}_+ and \mathcal{O}_- . It is easy to check that χ_- fixed point shares the same scaling dimensions of T_{ij}^p and B_i with those of χ_+ fixed point. The only change in scaling dimension is that

$$\begin{aligned}\Delta(T_{10}^s) &= \Delta(T_{02}^s) = \frac{2K_0 + K_+ + K_-}{1 + K_-(2K_0 + K_+)} \\ \Delta(T_{01}^s) &= \Delta(T_{20}^s) = 0\end{aligned}\quad (147)$$

Therefore, when Eq. 143 is satisfied, both χ_+ and χ_- fixed points are stable. In other words, χ_+ and χ_- fixed points coexist, and we expect an interesting intermediate unstable fixed point which characterizes the phase transition between these two fixed points.

M5. A_0 fixed point

Asymmetric fixed point A_i takes place when channel i is disconnected to the rest of the junction, while the other two channels are fully connected via electron tunneling process. For A_0 fixed point, B_0 and T_{12}^p will have vanishing scaling dimension, with

$$\mathcal{O}_{A_0} = \begin{pmatrix} -1 & 0 & 0 \\ 0 & -1 & 0 \\ 0 & 0 & 1 \end{pmatrix}.\quad (148)$$

and

$$\phi_0 = \phi_+ = \theta_- = 0.\quad (149)$$

\mathcal{O}_{A_0} is obviously orthogonal. The scaling dimensions at this fixed point are

$$\begin{aligned}\Delta(T_{10}^s) &= \Delta(T_{01}^s) = \Delta(T_{02}^s) = \Delta(T_{20}^s) = \frac{1 + K_-(2K_0 + K_+)}{4K_-} \\ \Delta(T_{01}^p) &= 2K_0 + K_+ \\ \Delta(T_{12}^p) &= 0 \\ \Delta(T_{20}^p) &= 2K_0 + K_+ \\ \Delta(B_0) &= 0 \\ \Delta(B_1) &= \frac{1}{K_-} \\ \Delta(B_2) &= \frac{1}{K_-}.\end{aligned}\quad (150)$$

For $K_- < 1$, $B_{1,2}$ are always irrelevant under RG. Thus, A_0 fixed point is stable when

$$\begin{aligned}2K_0 + K_+ &> 4 - \frac{1}{K_-} \\ 2K_0 + K_+ &> 1\end{aligned}\quad (151)$$

Thus,

$$K_0 > \frac{C_{A_0} - K_+}{2}\quad (152)$$

where $C_{A_0} = \max\{1, 4 - \frac{1}{K_-}\}$.

M6. A_1 fixed point

For A_1 fixed point, we require T_{02}^s , T_{20}^s , T_{20}^p and B_1 possessing zero scaling dimension. It turns out that these conditions are compatible with each other, leading to rotation matrix

$$\mathcal{O}_{A_1} = \frac{1}{2K_0 + K_+ + K_-} \begin{pmatrix} 2K_0 - K_+ - K_- & -2\sqrt{2K_0K_+} & 2\sqrt{2K_0K_-} \\ -2\sqrt{2K_0K_+} & -2K_0 + K_+ - K_- & -2\sqrt{K_+K_-} \\ 2\sqrt{2K_0K_-} & -2\sqrt{K_+K_-} & -2K_0 - K_+ + K_- \end{pmatrix}.\quad (153)$$

Despite its complicated form, one can still check that $\mathcal{O}_{A_1} \mathcal{O}_{A_1}^T = 1$ is satisfied. We find that

$$\phi_0 = \sqrt{2}\phi_-, \quad \phi_+ = -\phi_-, \quad \theta_- + \sqrt{2}\theta_0 = \theta_+, \quad (154)$$

and

$$\begin{aligned} \Delta(T_{10}^s) &= \Delta(T_{01}^s) = \frac{1 + K_-(2K_0 + K_+)}{2K_0 + K_+ + K_-} \\ \Delta(T_{02}^s) &= \Delta(T_{20}^s) = 0 \\ \Delta(T_{01}^p) &= 4\left(\frac{1}{K_-} + \frac{1}{2K_0 + K_+}\right)^{-1} \\ \Delta(T_{12}^p) &= 4\left(\frac{1}{K_-} + \frac{1}{2K_0 + K_+}\right)^{-1} \\ \Delta(T_{20}^p) &= 0 \\ \Delta(B_0) &= \frac{4}{2K_0 + K_+ + K_-} \\ \Delta(B_1) &= 0 \\ \Delta(B_2) &= \frac{4}{2K_0 + K_+ + K_-}. \end{aligned} \quad (155)$$

Thus, A_1 fixed point is stable when

$$\begin{aligned} [1 - (2K_0 + K_+)](1 - K_-) &> 0 \\ \frac{1}{K_-} + \frac{1}{2K_0 + K_+} &< 4 \\ 2K_0 + K_+ + K_- &< 4 \end{aligned} \quad (156)$$

Thus,

$$\begin{aligned} \frac{(4 - \frac{1}{K_-})^{-1} - K_+}{2} &< K_0 < \frac{1 - K_+}{2} \\ K_- &> \frac{1}{4} \end{aligned} \quad (157)$$

M7. A_2 fixed point

For A_2 fixed point, the terms T_{01}^s , T_{10}^s , T_{01}^p and B_2 can carry zero scaling dimension simultaneously, giving rise to

$$\mathcal{O}_{A_1} = \frac{1}{2K_0 + K_+ + K_-} \begin{pmatrix} 2K_0 - K_+ - K_- & -2\sqrt{2K_0K_+} & -2\sqrt{2K_0K_-} \\ -2\sqrt{2K_0K_+} & -2K_0 + K_+ - K_- & 2\sqrt{K_+K_-} \\ -2\sqrt{2K_0K_-} & 2\sqrt{K_+K_-} & -2K_0 - K_+ + K_- \end{pmatrix}. \quad (158)$$

and

$$\phi_0 = -\sqrt{2}\phi_-, \quad \phi_+ = \phi_-, \quad \theta_- + \theta_+ = \sqrt{2}\theta_0. \quad (159)$$

Then

$$\begin{aligned}
\Delta(T_{10}^s) &= \Delta(T_{01}^s) = 0 \\
\Delta(T_{02}^s) &= \Delta(T_{20}^s) = \frac{1 + K_-(2K_0 + K_+)}{2K_0 + K_+ + K_-} \\
\Delta(T_{01}^p) &= 0 \\
\Delta(T_{12}^p) &= 4\left(\frac{1}{K_-} + \frac{1}{2K_0 + K_+}\right)^{-1} \\
\Delta(T_{20}^p) &= 4\left(\frac{1}{K_-} + \frac{1}{2K_0 + K_+}\right)^{-1} \\
\Delta(B_0) &= \frac{4}{2K_0 + K_+ + K_-} \\
\Delta(B_1) &= \frac{4}{2K_0 + K_+ + K_-} \\
\Delta(B_2) &= 0.
\end{aligned} \tag{160}$$

Thus, A_2 fixed point is stable when

$$\begin{aligned}
[1 - (2K_0 + K_+)](1 - K_-) &> 0 \\
\frac{1}{K_-} + \frac{1}{2K_0 + K_+} &< 4 \\
2K_0 + K_+ + K_- &< 4
\end{aligned} \tag{161}$$

It is easy to see that A_1 and A_2 fixed points coexist in the same parameter region.

M8. Majorana-free phase diagram without bulk pair-hopping interaction

Now we are ready to map out the phase diagram of DSM nanowire junction without pair-hopping interaction (Majorana-free). As shown in Fig. 5, the phase diagrams are plotted for a fixed K_- value in: (a) $K_- = 0.4$, (b) $K_- = 0.6$, (c) $K_- = 0.8$, (d) $K_- = 1$. Remarkably, the junction is at stable asymmetric A_0 fixed point in the ‘‘free fermion’’ limit with $K_0 = K_+ = 1$ (red dot), where wire $i = 0$ is completely disconnected from wire $i = 1, 2$. In this weakly interacting region with $K_- < 1$, the two-terminal conductance across the junction should be zero.

APPENDIX N. PHASE DIAGRAM OF 2LL/LL JUNCTION WITH RMZM

When bulk pair-hopping interaction is incorporated between channel $i = 1$ and $i = 2$, there exists a rMZM bound state at the 2LL/LL junction. Pair-hopping interaction g pins θ_- to a classical value $\sqrt{\pi}n_{\theta_-}$, with $n_{\theta_-} \in \mathbb{Z}$. Interestingly, it is possible that certain boundary condition pins ϕ_- to $\sqrt{\pi}n_{\phi_-}x$ ($n_{\phi_-} \in \mathbb{Z}$) simultaneously at $x = 0$, even though θ_- and ϕ_- do NOT commute with each other. Such competition between bulk interaction and boundary condition requires promoting both n_{ϕ_-} and n_{θ_-} to integer-valued operators to recover the non-commutativity between ϕ_- and θ_- at $x = 0$. With this subtlety, we briefly summarize our strategy to study the critical behaviors here:

(1) For a generic tunneling/backscattering operator $t = \cos \sqrt{\pi}[(m_0\phi_0 + m_+\phi_+ + m_-\phi_-) + (n_0\theta_0 + n_+\theta_+ + n_-\theta_-)]$. The pinning of θ_- is equivalent to setting $n_- = 0$ in t in RG calculation.

(2) With $n_- = 0$, we force $\Delta(t)$ (the scaling dimension of t) to be zero to arrive at a possible fixed point F_t , which is characterized by an \mathcal{O}_t matrix. **F_t is a physical fixed point with $\Delta(t) = 0$, only if orthogonality condition $\mathcal{O}_t^T \mathcal{O}_t = 1$ is still satisfied. Otherwise, F_t is not physical and does not show up in the phase diagram.**

(3) Write down the explicit boundary conditions of a physical fixed point, and check that whether the boundary condition forces the pinning of ϕ_- . **If pinning of ϕ_- is not required by the boundary condition, any operator t with $m_- \neq 0$ is forced to vanish due to strong ϕ_- fluctuations and does not enter the phase diagram.**

(4) Use \mathcal{O}_t to calculate the remaining perturbation terms, and obtain the stability condition of F_t .

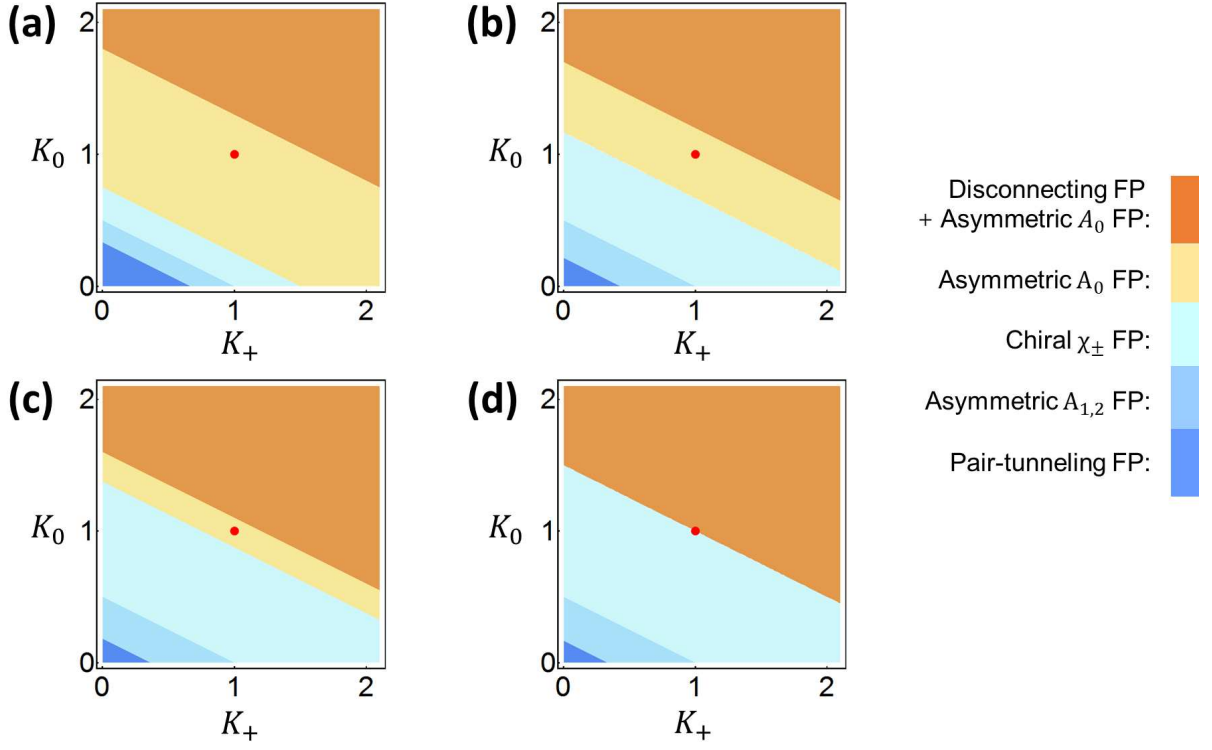


FIG. 5. Majorana-free phase diagram with K_- value: (a) $K_- = 0.4$, (b) $K_- = 0.6$, (c) $K_- = 0.8$, (d) $K_- = 1$

N1. Why χ_+ fixed point is not physical in 2LL/LL junction with rMZM?

To start with, we apply the above criterion to χ_+ fixed point, and explicitly show that in the presence of pair hopping interaction g , the rotation matrix of χ_+ fixed point \mathcal{O}_+ is modified to a non-orthogonal form $\mathcal{O}_+^{(g)}$. Recall that χ_+ fixed point forces trivial scaling dimensions of T_{10}^s and T_{02}^s . Let us first write down

$$\begin{aligned}
 T_{10}^s &\sim \cos \sqrt{\pi} \left[\frac{\tilde{\chi}_{0,L} + \tilde{\chi}_{0,R}}{2\sqrt{K_0}} + \frac{\sqrt{K_0}}{2} (\tilde{\chi}_{0,L} - \tilde{\chi}_{0,R}) + \frac{\tilde{\chi}_{+,L} + \tilde{\chi}_{+,R}}{2\sqrt{2K_+}} - \frac{\sqrt{K_+}}{2\sqrt{2}} (\tilde{\chi}_{+,L} - \tilde{\chi}_{+,R}) + \frac{\tilde{\chi}_{-,L} + \tilde{\chi}_{-,R}}{2\sqrt{2K_-}} \right] \\
 T_{02}^s &\sim \cos \sqrt{\pi} \left[\frac{\tilde{\chi}_{0,L} + \tilde{\chi}_{0,R}}{2\sqrt{K_0}} - \frac{\sqrt{K_0}}{2} (\tilde{\chi}_{0,L} - \tilde{\chi}_{0,R}) + \frac{\tilde{\chi}_{+,L} + \tilde{\chi}_{+,R}}{2\sqrt{2K_+}} + \frac{\sqrt{K_+}}{2\sqrt{2}} (\tilde{\chi}_{+,L} - \tilde{\chi}_{+,R}) - \frac{\tilde{\chi}_{-,L} + \tilde{\chi}_{-,R}}{2\sqrt{2K_-}} \right] \quad (162)
 \end{aligned}$$

where we have ignored the constant part originated from the pinning of θ_- . Together with the current conservation condition, the existence of χ_+ fixed point requires the following equations to be satisfied

$$\begin{aligned}
 \frac{\tilde{\chi}_{0,R} + \tilde{\chi}_{0,L}}{\sqrt{2K_0}} + \frac{\tilde{\chi}_{+,R} + \tilde{\chi}_{+,L}}{\sqrt{K_+}} &= 0 \\
 \frac{\tilde{\chi}_{0,R} + \tilde{\chi}_{0,L}}{\sqrt{K_0}} + \frac{\tilde{\chi}_{+,R} + \tilde{\chi}_{+,L}}{\sqrt{2K_+}} &= 0 \\
 \sqrt{K_0}(\tilde{\chi}_{0,L} - \tilde{\chi}_{0,R}) - \frac{\sqrt{K_+}}{\sqrt{2}}(\tilde{\chi}_{+,L} - \tilde{\chi}_{+,R}) + \frac{\tilde{\chi}_{-,L} + \tilde{\chi}_{-,R}}{\sqrt{2K_-}} &= 0 \quad (163)
 \end{aligned}$$

This immediately leads to the following solution

$$\begin{aligned}
 \tilde{\chi}_{0,R} &= -\tilde{\chi}_{0,L}, \quad \tilde{\chi}_{+,R} = -\tilde{\chi}_{+,L} \\
 \tilde{\chi}_{-,R} &= -2\sqrt{2K_0K_-}\tilde{\chi}_{0,L} + 2\sqrt{K_+K_-}\tilde{\chi}_{+,L} - \tilde{\chi}_{-,L} \quad (164)
 \end{aligned}$$

Therefore, the rotation matrix is given by

$$\mathcal{O}_+^{(g)} = \begin{pmatrix} -1 & 0 & 0 \\ 0 & -1 & 0 \\ -2\sqrt{2K_0K_-} & 2\sqrt{K_+K_-} & -1 \end{pmatrix}. \quad (165)$$

It is easy to verify that $\mathcal{O}_+^{(g)}$ fails to satisfy the orthogonal condition. As a result, χ_+ fixed point is not physical in the presence of g , and should not be considered as a candidate of fixed point in the phase diagram. Similar argument can be performed to other fixed points, and we find that χ_{\pm} and $A_{1,2}$ fixed points are unphysical. The analysis of remaining physical fixed points are given below.

N2. Disconnecting fixed point

With $n_- = 0$, we find that the disconnecting fixed point is characterized by the same \mathcal{O}_D matrix,

$$\mathcal{O}_D = \begin{pmatrix} -1 & 0 & 0 \\ 0 & -1 & 0 \\ 0 & 0 & -1 \end{pmatrix}. \quad (166)$$

The explicit boundary condition is

$$\phi_0 = \phi_+ = \phi_- = 0, \quad (167)$$

where both ϕ_- and θ_- are pinned at $x = 0$. Therefore,

$$\begin{aligned} \Delta(T_{10}^s) &= \frac{1}{4}(2K_0 + K_+) \\ \Delta(T_{01}^s) &= \frac{1}{4}(2K_0 + K_+) \\ \Delta(T_{01}^p) &= 2K_0 + K_+ \\ \Delta(T_{12}^p) &= 0 \\ \Delta(T_{20}^p) &= 2K_0 + K_+ \\ \Delta(B_0) &= 0 \\ \Delta(B_1) &= 0 \\ \Delta(B_2) &= 0. \end{aligned} \quad (168)$$

Notice that the scaling dimensions have been modified compared with Eq. 133. Here $\Delta(T_{12}^p) = 0$ is a manifestation of pinning θ_- , which will also appear in other fixed points. Now, disconnecting fixed point is stable when

$$K_0 > \frac{4 - K_+}{2} \quad (169)$$

N3. Pair-tunneling fixed point

With $n_- = 0$, the \mathcal{O}_D matrix remain unchanged compared with the $n_- \neq 0$ case. Thus, we still have

$$\phi_0 = -\sqrt{2}\phi_+, \quad \theta_+ = \sqrt{2}\theta_0, \quad \theta_- = 0, \quad (170)$$

where ϕ_- is not pinned by the boundary condition, and thus will be strongly fluctuating due to the pinning of θ_- . Therefore, terms that involve ϕ_- , such as T_{\pm}^s and $B_{1,2}$, will vanish under RG. The only allowed perturbation term at this fixed point is the backscattering term B_0 , with

$$\Delta(B_0) = \frac{4}{2K_0 + K_+} \quad (171)$$

So, pair-tunneling fixed point is stable when

$$K_0 < \frac{4 - K_+}{2} \quad (172)$$

Comparing this stability condition with Eq. 169, we find that disconnecting fixed point and pair-tunneling fixed point are dual to each other.

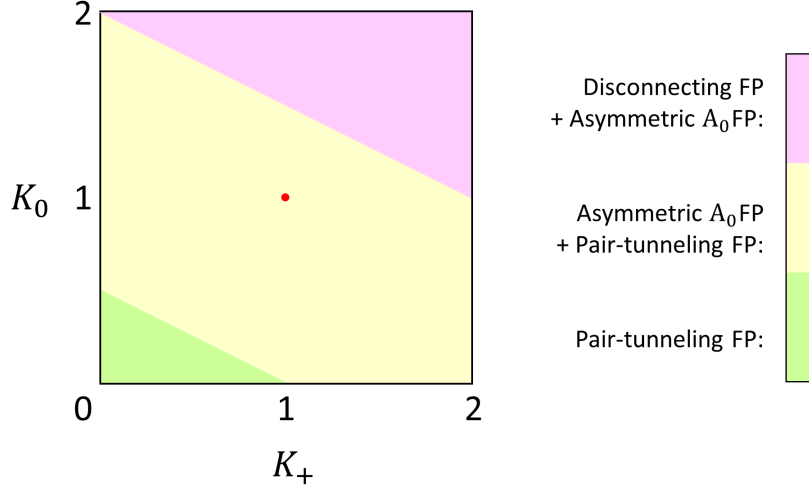


FIG. 6. The phase diagram with rMZM (pair hopping interaction).

N4. A_0 fixed point

For asymmetric fixed point A_0 , \mathcal{O}_{A_0} remains the same with or without the pinning condition $n_- = 0$. The explicit boundary condition is

$$\phi_0 = \phi_+ = \theta_- = 0. \quad (173)$$

Then ϕ_- is also strongly fluctuating, and the non-vanishing tunneling processes are pair-tunneling T_{01}^p and T_{20}^p , with

$$\Delta(T_{01}^p) = \Delta(T_{20}^p) = 2K_0 + K_+ \quad (174)$$

Thus, A_0 fixed point is stable when

$$2K_0 + K_+ > 1 \quad (175)$$

N5. Phase diagram with rMZM

The phase diagram can be easily mapped out in Fig. 6, and quite remarkably, the phase boundaries are completely independent of the value of K_- , in comparison with Fig. 5. As shown in Fig. 6, in the weak interacting region, the DSM nanowire junction is in the coexisting phase between A_0 fixed point and pair-tunneling fixed point. This signals the emergence of an unstable fixed point which characterizes the phase transition between A_0 fixed point and pair-tunneling fixed point, which is similar to a pinch-off transition.

APPENDIX O. A FURTHER LOOK AT THE \mathcal{O} MATRIX

In the previous section, we have successfully mapped out the tunneling phase diagrams of the 2LL/LL junction with and without the pair-hopping interaction. The key information of each tunneling phase is encoded in the orthogonal matrix \mathcal{O} . Interestingly, the form of \mathcal{O} of three-wire-junctions has been discussed in earlier literatures [49–52] under very general assumptions. In particular, it has been shown that \mathcal{O} matrices could be classified into two different classes based on whether their determinant is +1 or -1:

- When $\det \mathcal{O} = -1$, \mathcal{O} corresponds to a fixed point that possesses a Z_3 symmetry among the three quantum wires. For example, at the disconnecting fixed point (DFP), every quantum wire is in the strong backscattering limit. If we relabel the wire indices at DFP, the DFP physics will not be affected and thus possesses the Z_3 symmetry among three quantum wires. Other fixed points that belong to this class are: pair-tunneling fixed point and chiral χ_{\pm} fixed points.

	DFP	χ_+ FP	χ_- FP	PFP	A ₀ FP	A ₁ FP	A ₂ FP
\mathcal{O} :	\mathcal{O}_D	\mathcal{O}_+	\mathcal{O}_-	\mathcal{O}_P	\mathcal{O}_{A_0}	\mathcal{O}_{A_1}	\mathcal{O}_{A_2}
\mathcal{S} :	$\mathcal{S}^{(1)}(t=0)$	$\mathcal{S}^{(1)}(t=-\frac{2\pi}{3})$	$\mathcal{S}^{(1)}(t=\frac{2\pi}{3})$	$\mathcal{S}^{(1)}(t=-\pi)$	$\mathcal{S}^{(2)}(t=\pi)$	$\mathcal{S}^{(2)}(t=\frac{\pi}{3})$	$\mathcal{S}^{(2)}(t=-\frac{\pi}{3})$

TABLE III. In this table, we applied Eq. 180 and established the mapping between \mathcal{O} matrices we found using DEBC method in our 2LL/LL junction and the \mathcal{S} matrices defined in Ref. [51].

- When $\det \mathcal{O} = +1$, \mathcal{O} corresponds to a fixed point that explicitly breaks the Z_3 symmetry among the three quantum wires. The asymmetric fixed points $A_{0,1,2}$ belong to this class. If we start from A_0 FP and relabel the wire indices in the following way: $0 \rightarrow 1, 1 \rightarrow 2, 2 \rightarrow 0$, we will arrive at the A_1 FP. Therefore, A_0 FP, as well as A_1 and A_2 FP, explicitly breaks the Z_3 symmetry.

To compare with the results in Ref. [51, 52], we first notice that there are three important differences between the notations:

1. In Ref. [51], the three quantum wires share the same Luttinger parameter g . While in our model, we have assumed the Luttinger parameters K_0 and K_{\pm} to be different from each other.
2. In our theory, we have performed a unitary transformation to the dual boson fields, and rotate $\phi_{1,2}$ and $\theta_{1,2}$ into the bonding/anto-bonding basis ϕ_{\pm} and θ_{\pm} :

$$U = \begin{pmatrix} 1 & 0 & 0 \\ 0 & \frac{1}{\sqrt{2}} & \frac{1}{\sqrt{2}} \\ 0 & \frac{1}{\sqrt{2}} & -\frac{1}{\sqrt{2}} \end{pmatrix} \quad (176)$$

3. The bosonization convention in our work is different from that of earlier works:

$$\psi_{l,R} \sim e^{i\phi_{l,O}} \sim e^{i\sqrt{\pi}\chi_{l,R}}, \quad \psi_{l,L} \sim e^{i\phi_{l,I}} \sim e^{-i\sqrt{\pi}\chi_{l,L}} \quad (177)$$

where $\phi_{l,O/I}$ and $\chi_{l,R/L}$ are the chiral bosons defined in Ref. [51] and in our work, respectively. As a result, we have

$$\phi_{l,O} = \sqrt{\pi}\chi_{l,R}, \quad \phi_{l,I} = -\sqrt{\pi}\chi_{l,L}. \quad (178)$$

As a comparison, we follow the convention of Ref. [51] and denote the orthogonal matrix that connects ϕ_O and ϕ_I as \mathcal{S} . Ref. [51] showed the explicit expressions of \mathcal{S} matrix parametrized by a single angular variable $t \in [-\pi, \pi)$ at $g = 1$:

$$\begin{aligned} \mathcal{S}^{(1)}(t) &= \frac{1}{3} \begin{pmatrix} 1 + 2 \cos t & 1 - \cos t + \sqrt{3} \sin t & 1 - \cos t - \sqrt{3} \sin t \\ 1 - \cos t - \sqrt{3} \sin t & 1 + 2 \cos t & 1 - \cos t + \sqrt{3} \sin t \\ 1 - \cos t + \sqrt{3} \sin t & 1 - \cos t - \sqrt{3} \sin t & 1 + 2 \cos t \end{pmatrix} \\ \mathcal{S}^{(2)}(t) &= \frac{1}{3} \begin{pmatrix} 1 - 2 \cos t & 1 + \cos t - \sqrt{3} \sin t & 1 + \cos t + \sqrt{3} \sin t \\ 1 + \cos t - \sqrt{3} \sin t & 1 + \cos t + \sqrt{3} \sin t & 1 - 2 \cos t \\ 1 + \cos t + \sqrt{3} \sin t & 1 - 2 \cos t & 1 + \cos t - \sqrt{3} \sin t \end{pmatrix} \end{aligned} \quad (179)$$

where $\mathcal{S}^{(1)}$ with $\det \mathcal{S}^{(1)} = +1$ and $\mathcal{S}^{(2)}$ with $\det \mathcal{S}^{(2)} = -1$ denote the Z_3 -symmetric and Z_3 -asymmetric classes, respectively. Based on our previous analysis, by taking $K_0 = K_+ = K_- = 1$ and performing a unitary transformation, we are able to map our \mathcal{O} matrices found in the previous sections to the $\mathcal{S}^{(1)}$ and $\mathcal{S}^{(2)}$:

$$-(U\mathcal{O}_{\alpha}U^{-1})|_{K_0=K_{\pm}=1} = \mathcal{S}^{(\beta)}(t) \quad (180)$$

where α is the subscript for \mathcal{O} matrix depending on which fixed point we are talking about. $\beta = 1, 2$ is the superscript for \mathcal{S} matrix. The minus sign in Eq. 180 comes from the definition of $\phi_{l,I}$ in Eq. 178. Here we would like to point out that \mathcal{O}_{α} and $\mathcal{O}_{\alpha}|_{K_0=K_{\pm}=1}$ only differ by a field rescaling process in the definition. Therefore, it is sufficient to discuss the relationship between the non-interacting limit of \mathcal{O}_{α} and $\mathcal{S}^{(\beta)}$, which contains all of the key information. With Eq. 180, we have mapped all \mathcal{O} matrices to the corresponding \mathcal{S} matrices, and summarized these results in Table. III.